Journal of Medicinal Chemistry

Article

pubs.acs.org/jmc

Discovery of Highly Selective and Nanomolar Carbamate-Based Butyrylcholinesterase Inhibitors by Rational Investigation into Their Inhibition Mode

Edgar Sawatzky,[†] Sarah Wehle,[†] Beata Kling,[‡] Jan Wendrich,[§] Gerhard Bringmann,[§] Christoph A. Sotriffer,[†] Jörg Heilmann,[‡] and Michael Decker*[,†]

[†]Pharmazeutische und Medizinische Chemie, Institut für Pharmazie und Lebensmittelchemie, Universität Würzburg, Am Hubland, D-97074 Würzburg, Germany

[‡]Lehrstuhl für Pharmazeutische Biologie, Institut für Pharmazie, Universität Regensburg, Universitätsstraße 31, D-93053 Regensburg, Germany

[§]Lehrstuhl für Organische Chemie I, Institut für Organische Chemie, Universität Würzburg, Am Hubland, D-97074 Würzburg, Germany

Supporting Information

ABSTRACT: Butyrylcholinesterase (BChE) is a promising target for the treatment of later stage cognitive decline in Alzheimer's disease. A set of pseudo-irreversible BChE inhibitors with high selectivity over *h*AChE was synthesized based on carbamates attached to tetrahydroquinazoline scaffolds with the 2-thiophenyl compound **2p** as the most potent inhibitor of *eq*BChE (K_C = 14.3 nM) and also of *h*BChE (K_C = 19.7 nM). The inhibitors transfer the carbamate moiety onto the active site under release of the phenolic tetrahydroquinazoline scaffolds that themselves act as neuroprotectants. By combination of kinetic data with molecular docking studies, a plausible binding model was probed describing how the tetrahydroquinazoline scaffold guides the carbamate into a close position to the active site. The model explains the influence of the carrier scaffold onto the affinity of an inhibitor just before carbamate transfer. This strategy can be used to utilize the binding mode of other carbamate-based inhibitors.

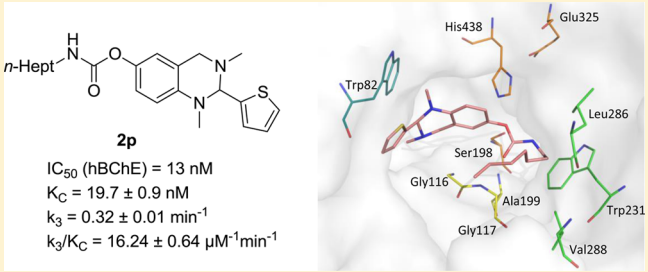

INTRODUCTION

In 2010 the World Alzheimer Report[1,2] estimated the worldwide societal costs of dementia to a value of 604 billion dollars with an increase of prevalence from 35 million people in 2010 to 115 million people in 2050. The most common form of dementia is Alzheimer's disease (AD), a progressive neurodegenerative disorder of multifactorial nature characterized by the loss of cognitive abilities through the death of central neuronal cells.

Although the initial pathophysiological reasons in AD are still not yet fully understood, the pathogenesis is mainly determined by several specific biochemical changes,[3,4] namely, (i) aggregation of toxic β-amyloid oligomers[5,6] followed by deposition of larger insoluble fibers in advanced amyloid plaques,[7] (ii) hyperphosphorylation of tau proteins and their aggregation into toxic neurofibrillary tangles,[8−10] (iii) oxidative stress with subsequent cell death,[11,12] and (iv) the imbalance of the two major neurotransmitters acetylcholine (ACh) and glutamate which are necessary for cognition.[13−15] Although these multifactorial changes provide a broad spectrum of possible therapeutic targets, there are only four approved drugs on the market, all targeting the neurotransmitter systems. The non-competitive antagonist memantine targets the glutamatergic system through binding at the ionotropic glutamate receptor NMDA. Besides, the cholinergic system is affected by the acetylcholinesterase (AChE) inhibitors rivastigmine, donezepil, and galantamine. Several clinical studies on these cholinesterase inhibitors[16−18] have proven their positive effectiveness with regard to cognition, global cognitive functions, and daily activities, but due to their (only) symptomatic mode of action, no curative treatment is achieved.

The decline of cognition during AD is attributed to the progressive loss of cholinergic neurons and therefore to a deficit of ACh. This deficit is permanently enhanced through the decomposition of available ACh in the synaptic gap of neuronal cells by AChE that normally regulates the amount of ACh in healthy brain. Therefore, inhibition of AChE can compensate the lack of ACh and in consequence improve cognitive abilities. In advanced AD the level of AChE drops down to 90% compared to the healthy brain,[19−21] making it impractical as a target for therapeutic use in later stages of AD. Clinical trials are in striking accordance with the lack of effectiveness of AChE inhibitors in these stages of AD. On the other hand, several studies[20−23] have shown increased levels of the isoenzyme butyrylcholinesterase

Received: October 26, 2015

DOI: 10.1021/acs.jmedchem.5b01674
J. Med. Chem. XXXX, XXX, XXX−XXX

(BChE) in AD patients in brain areas that are relevant for cognition. Although the role of BChE for ACh hydrolysis in healthy brain is only of minor impact, there is strong evidence that BChE compensates the loss of neuronal AChE in progressed AD and therefore takes over the function of AChE. This hypothesis is supported by an AChE knockout mouse model[24] in which mice did not suffer on cholinergic hyperactivation in the absence of AChE as ACh hydrolysis is controlled by BChE. These data are in agreement with other reports[18,25−28] showing a positive correlation between selective BChE inhibition, improved cognitive performance, and memory acquisition. In a recent in vivo study with BChE knockout mice it was shown that in contrast to wild-type mice, lipid peroxidation and ACh levels were not changed after treatment with amyloid-β_{25-35} and learning capacities were attenuated.[28] Therefore, inhibition of BChE might well constitute a therapeutic target for clinical use in progressed AD, where AChE inhibitors fail.

And further, BChE might be of clinical interest not only for AD treatment, as it was found to be involved in the regulation of the serum metabolism in context with obesity,[29,30] insulin resistance and diabetes mellitus,[30,31] and cardiovascular risk factors.[32,33] Accordingly, for investigation into the role of BChE in these research fields, the search for highly active and selective inhibitors and their development are of high importance.

Selective targeting of BChE over AChE is a challenging task, as sequence comparison of the two isoforms *h*AChE and *h*BChE shows an identity of 49% and a similarity of 66% (see Supporting Information). Although the catalytic active site (CAS), where hydrolysis of the neurotransmitter is mediated,[34] of both enzymes is highly conserved, the two enzymes show differences in the space they provide for a substrate or inhibitor, respectively. These differences are notably seen in the amino acids forming the gorge of the binding site and the acyl binding pocket (for a more detailed comparison see ref 35).

However, selective inhibition of BChE can be achieved by targeting the CAS with carbamate-based inhibitors. These inhibitors generally feature a carrier scaffold guiding a carbamate moiety into the correct position in the enzyme, successively followed by the transfer of the carbamate moiety onto the serine of the CAS under release of the carrier scaffold (see Figure 1). In the literature the development of pseudo-irreversible ChE inhibitors is in most cases limited to the modification of the transferable carbamate moiety,[36−39] but at the current stage only very limited information with regard to the binding mode of the carrier scaffold itself is available (Figure 1).[40−43]

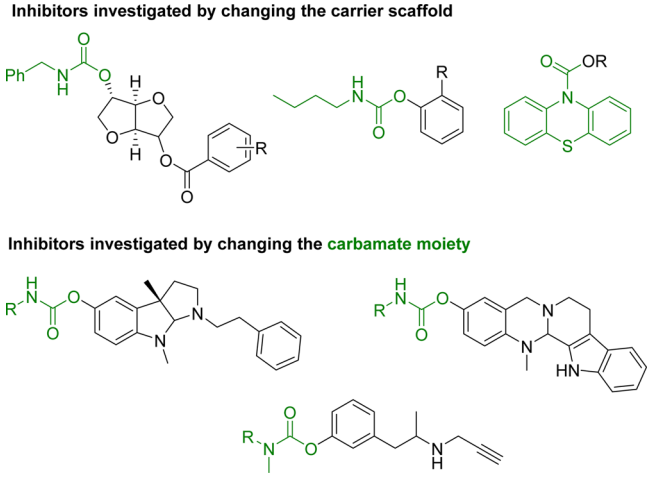

Figure 1. Previously described carbamate-based structures investigated as ChE inhibitors by altering the carrier scaffold[40,42,43] (top) and by altering the carbamate moiety.[36−38] Carrier scaffolds are shown in black, carbamate moieties in green.

For rational design of carbamate-based BChE inhibitors there is a strong requirement for enhanced knowledge of the interactions between the carrier scaffold and the enzyme. Only a well bound carrier in the correct position offers the possibility for carbamate transfer and thus for enzyme inhibition. Concise knowledge about an appropriate experimental approach will of course also be useful for the development of other types of pseudo-irreversible inhibitors. Surprisingly, to our knowledge such experimental investigations are lacking to a large degree. In the present study we designed, synthesized, and investigated a set of bicyclic compounds as selective BChE inhibitors to explore the binding mode of the carrier scaffold into the active center of BChE by chemical modifications of the carrier scaffold. Subsequently and in part parallel to these efforts, a molecular docking model was established that describes a suitable binding mode.

Starting point of our investigation were tetrahydroquinazoline-derived scaffolds that can be used as templates for the synthesis of potent AChE and BChE inhibitors.[44−48] Further incorporation of a carbamate moiety into these molecular templates resulted in highly selective and nanomolar active BChE inhibitors with the tetracyclic *n*-heptyl carbamate **1** as the most potent one (Figure 2a).[36,47] This inhibitor binds to the active site of BChE with its tetrahydroquinazoline scaffold followed by the pseudo-irreversible transfer of the carbamate moiety onto the serine of the CAS ("pseudo" because the carbamate moiety slowly hydrolyzes off from the serine and enzyme activity is reconstituted). In consequence, this mode of action leads to release of the heterocyclic carrier scaffold which itself acts with its *p*-aminohydroquinoline moiety as an antioxidant preventing oxidative-stress-induced cell death (Figure 2b).[36,47]

Since the tetracyclic moiety of compound **1** is difficult to be modified comprehensively and systematically in a chemical sense with regard to SARs, the tetrahydroquinazoline-based scaffold was "opened" to access compound series **2** and **3** (Figure 2a), which enables the conduction of SARs. These compounds can be modified at the aryl residue site, and they can also be further exploited by introduction of suitable bulky *N*-site groups. In a previous study,[47] we had already investigated the role of the carbamate moiety on BChE inhibition by introducing the carbamate group of several known selective BChE inhibitors, like eptastigmine bearing a *n*-heptyl residue, rivastigmine bearing an ethylmethyl residue, or cymserine bearing a 4-*i*-Pr-phenyl residue at the carbamate site. We found that a *n*-heptyl residue incorporated into the carrier scaffold leads to the most affine and BChE-selective inhibitor in this series (compound **1**), and therefore we decided for compound series **2** and **3** to keep this residue constant for SAR investigations.[47]

With the target structures synthesized we performed kinetic studies to evaluate the mode of action and computational studies. We combined the kinetic data with the molecular docking studies and established a model for binding of these inhibitors to the enzyme. This model describes the binding mode of the tetrahydroquinazoline scaffolds just before carbamate transfer occurs onto BChE and therefore explains altered affinity and potency of these inhibitors based on the carrier scaffold. The scaffolds themselves take only little part in BChE inhibition, but they are guiding the carbamate moiety into the correct position

DOI: 10.1021/acs.jmedchem.5b01674
J. Med. Chem. XXXX, XXX, XXX−XXX

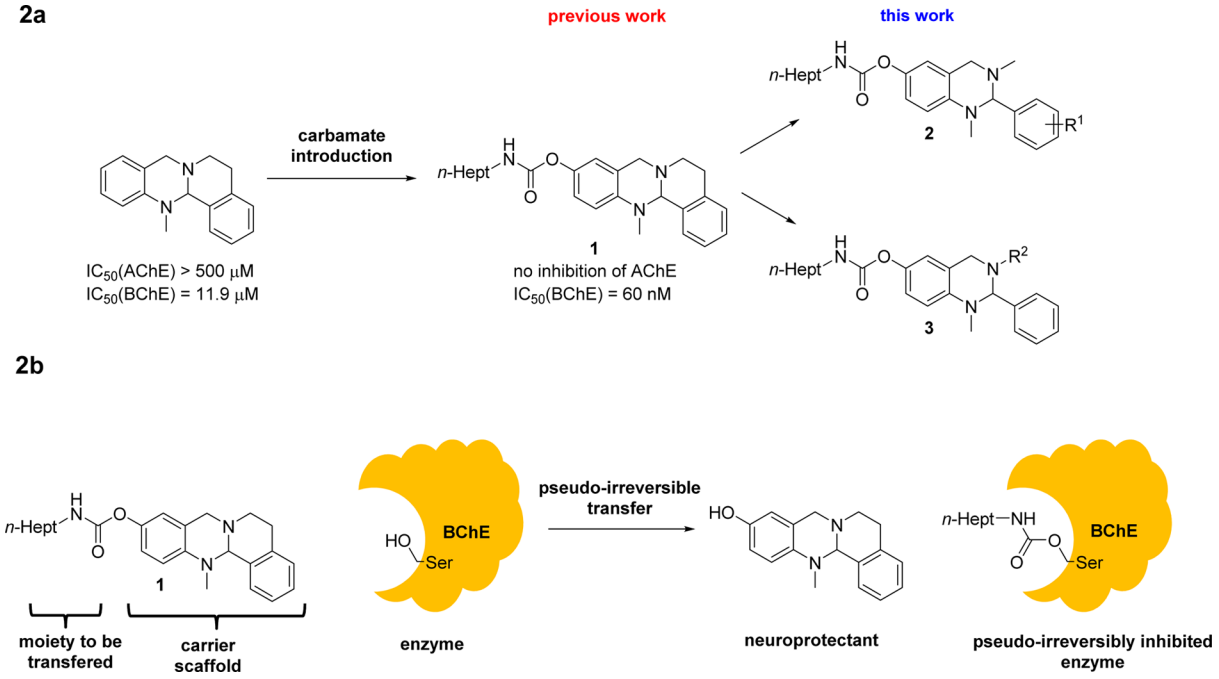

Figure 2. (a) Development of carbamate-based inhibitor **1** and modifications toward compounds **2** and **3** for SAR investigations of tetrahydroquinazoline-based carbamates. (b) Mode of inhibition of BChE by tetrahydroquinazoline-based carbamate **1**.[47]

Scheme 1. Synthesis of Aryl and *N*-Alkyl Substituted Target Compounds 2a−u and 3a−c[a]

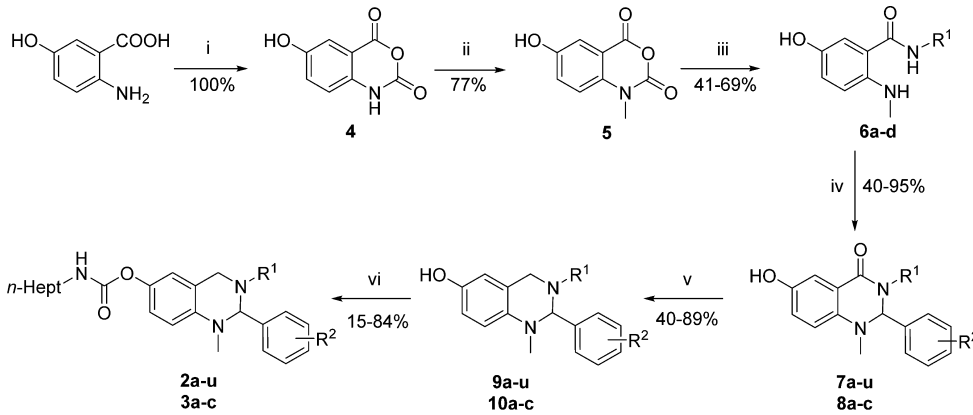

[a]For substitution pattern of R^1 and R^2 see Table 1. Reagents and conditions: (i) $CO(OCCl_3)_2$, THF, 70 °C, 3.5 h; (ii) MeI, DIPEA, DMAc, 40 °C, 24 h; (iii) R^1-NH_2 or $MeNH_3Cl$ and Et_3N, DMF, 40−120 °C, 4−5 h; (iv) R^2-PhCHO, AcOH, 70 °C, 1−3 h; (v) $LiAlH_4$, THF, reflux, 1−3 h; (vi) $(4\text{-}NO_2)PhO(C{=}O)NH$*n*-Hept , NaH, THF, rt, 2 h or *n*-Hept-NCO, Et_3N, rt, 6 h for **2o,p**.

toward the active site to enable carbamate transfer and therefore enzyme inhibition. By application of this general strategy, the binding mode of carbamate based inhibitors bearing transferable moieties can easily be investigated also for other biological targets through the combination of kinetic data and computational studies. This is possible as the general mechanism for carbamate-based pseudo-irreversible inhibitors is similar for all targets.

RESULTS AND DISCUSSION

Chemistry. Tetrahydroquinazoline substituted carbamates of the series **2** and **3** were synthesized as outlined in Scheme 1. The first two steps were described recently.[49] Briefly, 3-hydroxyanthranilic acid and triphosgene were heated in THF to yield 6-hydroxyisatoic anhydride **4** quantitatively. Subsequently, the selective N-methylation yielded compound **5**. Free amines or corresponding hydrochlorides were used to synthesize amides **6a−d** in moderate yields. These amides were cyclized with either benzaldehyde or substituted derivatives to yield dihydroquinazolinones **7a−u** and **8a−c** which were reduced with $LiAlH_4$ to give tetrahydroquinazolines **9a−u** and **10a−c**, respectively. In the last step, the *n*-heptyl carbamate moiety bearing compounds **2a−u** and **3a−c** were synthesized using 4-nitrophenyl-*n*-heptylcarbamate instead of the previously applied commercially available *n*-heptyl isocyanate, as its use led in some cases to the formation of the symmetric *n*-heptylurea which is difficult to remove.

Besides the target compounds above, also the fully aromatic compound **16** was synthesized in six steps (Scheme 2). 5-Hydroxy-2-nitrobenzaldehyde was *O*-benzyl protected, then the nitro moiety was reduced with iron using a catalytical amount of conc HCl solution toward **12**, and finally the amide bond of **13** was formed with benzoyl chloride. The cyclization was achieved

DOI: 10.1021/acs.jmedchem.5b01674
J. Med. Chem. XXXX, XXX, XXX−XXX

Scheme 2. Synthesis of Quinazoline 16[a]

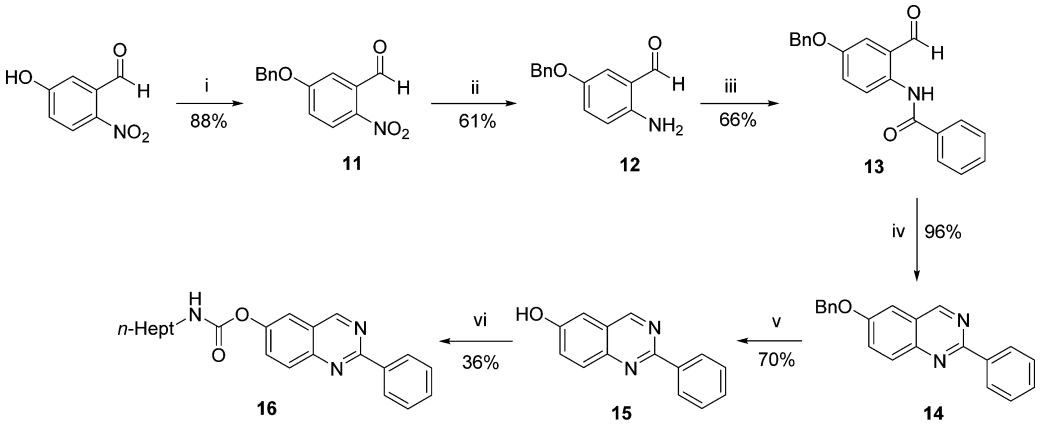

[a]Reagents and conditions: (i) BnBr, K_2CO_3, DMF, 40 °C, 24 h; (ii) Fe, HCl, EtOH/H_2O, reflux, 1 h; (iii) Ph(C═O)Cl, Et_3N, DCM, rt, 4 h; (iv) conc NH_3, *i*-PrOH, MW, 90 °C, 6 h; (v) Pd/C, H_2, MeOH, 50 °C, 3 h; (vi) (4-NO_2)PhO(C═O)NH*n*-Hept , NaH, THF, rt, 2 h.

Table 1. Cholinesterase Inhibition of the Synthesized Test Compounds[a]

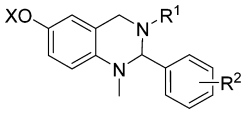

		IC_{50} [μM] or % inhibition			IC_{50} [μM] or % inhibition	
moiety	X = H	*eq*BChE	*h*AChE	X = (C═O)NH*n*-Hept	*eq*BChE	*h*AChE
R^1 = Me; R^2 =						
H	**9a**	39.9	327.0	**2a**	0.106	4%[d]
4-Cl-Ph-	**9b**	13.8	235.6	**2b**	0.115	24%[d]
3-Cl-Ph-	**9c**	2.1	242.4	**2c**	0.096	39%[d]
2-Cl-Ph-	**9d**	56.0	60%[b]	**2d**	0.474	48%[e]
4-Me-Ph-	**9e**	22.6	109.9	**2e**	0.231	9%[d]
3-Me-Ph-	**9f**	17.4	437.0	**2f**	0.199	27%[d]
2-Me-Ph-	**9g**	92.4	143.4	**2g**	0.251	18%[e]
4-MeO-Ph-	**9h**	39.5	103.8	**2h**	0.875	14%[d]
3-MeO-Ph-	**9i**	7.8	61%[b]	**2i**	0.208	10%[d]
2-MeO-Ph-	**9j**	9.9	192.8	**2j**	0.238	47%[e]
4-F-Ph-	**9k**	58.9	143.4	**2k**	0.044	1.61
4-CF_3-Ph-	**9l**	64.6	nd[c]	**2l**	2.7	59%[d]
4-pyridyl-	**9m**	2.1	242.4	**2m**	0.723	16%[d]
3-pyridyl-	**9n**	70.7	61%[b]	**2n**	0.565	18%[d]
3-thiophenyl-	**9o**	193.7	52%[b]	**2o**	0.022	13%[d]
2-thiophenyl	**9p**	63.2	225.8	**2p**	0.014, 0.013[f]	0%[d]
3-furyl-	**9q**	196.1	341.7	**2q**	0.083	12%[d]
3-pyrrolyl-	**9r**	15.3	115.9	**2r**	0.023	0.852
1-naphthyl-	**9s**	2.8	341.7	**2s**	36.2	8%[e]
2-naphthyl-	**9t**	16.5	9%[c]	**2t**	0.374	5%[e]
2,6-dichloro	**9u**	7.1	13.5	**2u**	0.531	33%[e]
R^2 = Ph; R^1 =						
i-Pr-	**10a**	55.8	253.0	**3a**	0.021	33%[d]
n-Pr-	**10b**	22.8	279.3	**3b**	0.040	46%[d]
benzyl-	**10c**	14.8	16%[c]	**3c**	0.034	17%[e]
	15	98.1	20%[b]	**16**	1.8	22%[d]
				physostigmine	0.078	0.032

[a]Phenols were incubated for 4.5 min and carbamates for 30 min. Experiments were performed in triplicate at AChE from human erythrocytes and BChE from equine serum. [b−e]Percent inhibition at a concentration of [b]500 μM, [c]50 μM, [d]100 μM, [e]10 μM. Table with confidence intervals is available in Supporting Information. [f]Values determined at human BChE.

in a modified procedure[50] by treatment of **13** with ammonia in a sealed tube under microwave irradiation to obtain **14**. In the last steps the benzyl protection group was removed under standard conditions using Pd/C and H_2 and the carbamate moiety was formed with 4-nitrophenyl-*n*-heptylcarbamate as mentioned above to obtain the quinazoline-based carbamate **16**.

Enzyme Inhibition and SARs. For evaluation and quantification of enzyme inhibition, Ellman's spectrophotomet-

DOI: 10.1021/acs.jmedchem.5b01674
J. Med. Chem. XXXX, XXX, XXX−XXX

ric method[45,51,52] was applied using AChE from human erythrocytes (EC 3.1.1.7) and BChE from equine serum (EC 3.1.1.8). BChE from horse serum was chosen, as it shows a sequence identity of 90% and a homology of 94% compared to the human analog.[53] Acetylthiocholine and butyrylthiocholine were used as substrates for *h*AChE and *eq*BChE inhibition, respectively. In short, the enzymes were preincubated with different concentrations of the synthesized phenols for 4.5 min or the corresponding carbamates for 30 min to enable time-dependent carbamate transfer onto the serine of the active site, before substrate was added to determine the remaining enzyme activity.

Only few highly selective and potent BChE inhibitors are described in the literature (and even fewer with the carbamate structure; see Figure 1), and only limited information on SARs regarding the carrier scaffold is reported. Therefore, the aromatic system in the target compounds was systematically altered. The unsubstituted target structure **2a** was synthesized as the reference compound and tested for the inhibition of *h*AChE and *eq*BChE (Table 1). This structure is a highly potent inhibitor with an IC_{50} value of 106 nM on *eq*BChE and no significant inhibition on *h*AChE, proving its *eq*BChE selectivity. By contrast, its unsubstituted phenolic analog **9a** shows weak inhibition on *h*AChE with IC_{50} = 327 μM and a value of 39.9 μM for *eq*BChE inhibition, corresponding to an approximately 400-fold decrease in inhibition of *eq*BChE compared to the carbamate **2a**. These results already support the hypothesis that BChE inhibition mainly occurs by carbamate transfer and that the tetrahydroquinazoline scaffold is only the carrier for the carbamate moiety lacking pronounced inhibition of the enzyme. Therefore, in the subsequent SARs analysis only the carbamate based compounds (right columns of Table 1) will be discussed, as their phenolic carrier scaffolds showed no pronounced inhibition (left columns of Table 1) in most cases on neither enzyme.

Optimization of the substitution pattern of the aromatic moiety was conducted by various approaches starting with the Topliss tree approach.[54,55] Within this approach the hydrophobic, electronic, and steric properties of an aromatic system are systematically altered by the introduction of different substituents with the aim to improve activity toward a biological target. In our case the Topliss tree approach guided to the synthesis of Cl- (**2b–d**), Me- (**2e–g**), and MeO- (**2h–j**) substituted aromatic systems in ortho, meta, and para positions and finally to the 4-fluorine substituted system **2k**. Interestingly, none of these groups improved affinity except for the fluorinated compound **2k** with the fluorine atom as the smallest substituent in this series with IC_{50}(BChE) = 44 nM. Compound **2l** bearing a strong electron withdrawing 4-CF_3 group was synthesized although not being recommended in the classical Topliss tree approach and showed strongly decreased BChE inhibition by a factor of 25 (IC_{50} = 2.7 μM). In addition to the Topliss tree approach, bioisosteric replacements for the phenyl system were investigated with pyridines **2m–n** and thiophenes **2o–p**.[56,57] Surprisingly, the pyridyl residues as more polar bioisosteres of the phenyl residue decreased inhibition and the thiophene residues as less polar bioisosteres increased inhibition more than 5-fold to IC_{50}(BChE) of 22 nM for **2o** and 14 nM for **2p**. With regard to these results, further similarity replacements of the thiophenyl system were investigated leading to the furyl compound **2q** with decreased activity (IC_{50}(BChE) = 83 nM) and the pyrrolyl compound **2r** (IC_{50}(BChE) = 23 nM) with BChE inhibition similar to that of the thiophenyl compound **2o**. Finally, the phenyl system was replaced by sterically demanding aromatic substituents; here the 1-naphthyl and the 2-naphthyl substituted compounds **2s,t** were investigated. Interestingly, inhibition of BChE by the 1-naphthyl substituted compound **2s** dropped to IC_{50}(BChE) = 36.2 μM (i.e., by a factor of approximately 300 compared to reference compound **2a**). To further investigate steric influence on the affinity toward BChE, the 2,6-disubstituted chlorine compound **2u** was synthesized which has to undergo a twist caused by its ortho-substitution pattern, thus leading to a almost perpendicular arrangement of the aryl ring and the bicyclic core. This compound shows an IC_{50} value of 531 nM, which is lower than for all three monosubstituted chlorine compounds (**2b,c,d**).

Beyond the mentioned introduction of different substitution patterns into the aromatic system, also the space close to the tertiary nitrogen was exploited by the replacement of the methyl group with other side groups (**3a–c**) with the best results for the *i*-Pr group with IC_{50}(BChE) = 21 nM. For the bicyclic aromatic quinazoline **16** a strongly decreased inhibition was observed meaning that either a bent system or a more basic nitrogen within the core structure is necessary for binding, comparable to many AChE inhibitors.[58–61]

As the 2-thiophenyl compound **2p** was found to be the most potent and selective compound toward *eq*BChE, its potency on *h*BChE was also investigated. The IC_{50} value on *h*BChE was determined to 13 nM and is comparable to the one on *eq*BChE (14 nM), proving that the results obtained on *eq*BChE can be used as an approximation for *h*BChE.

Even if the IC_{50} values of the compounds described in Table 1 (a respective table with confidence intervals is provided in the Supporting Information) are a useful first hint to establish a binding model for these inhibitors, the inhibition mode of pseudo-irreversible inhibitors is much more complex. Therefore, a more detailed view into the kinetic mode of action is necessary to determine the influence of substituents on enzyme inhibition. At this point, it should also be mentioned that the inhibition curves of the weakest active compounds **2l**, **2s**, and **16** show a Hill slope of around 0.5 (data not shown). These slopes are remarkably different from those of all other inhibitors (slope of ≥1). This fact might be a strong hint for a different mode of action for these three inhibitors.

Kinetic Investigations into the Mode of BChE Inhibition. The mechanism of pseudo-irreversible enzyme inhibition by carbamates can be described by three pivotal steps as shown in Figure 3. First, the enzyme E forms a reversible enzyme–

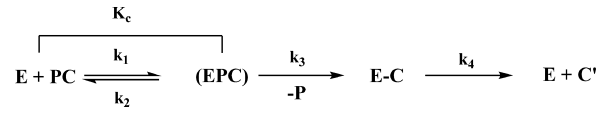

Figure 3. Pseudo-irreversible inhibition of an enzyme E by carbamates PC. For description see the main text.

inhibitor complex (EPC) with the carbamate-based inhibitor PC (PC for phenol carbamate) comparable to reversible competitive inhibitors. This reversible inhibition is quantified by K_C which describes the apparent affinity between the enzyme and the inhibitor in an equilibrium state. In the second step, the carbamate moiety itself is transferred onto the enzyme with release of the carrier scaffold P (P for phenol), resulting in the carbamoylated enzyme E–C. The constant k_3 represents the carbamolyation rate of the inhibitor from the reversible complex (EPC) to the carbamoylated enzyme E–C. The last step is the recovery of the enzyme through slow hydrolysis of E–C and

DOI: 10.1021/acs.jmedchem.5b01674
J. Med. Chem. XXXX, XXX, XXX–XXX

Table 2. Kinetic Values for Carbamoylation and Decarbamoylation on *eq*BChE for Selected Compounds[a]

	R^1	R^2	K_C [nM]	k_3 [min^{-1}]	k_3/K_C [$\mu M^{-1}min^{-1}$]	k_4 [h^{-1}]
2a	Me	Ph-	226.2 ± 82.8	0.13 ± 0.04	0.57 ± 0.27	0.14 ± 0.003
2p	Me	2-thiophenyl-	14.3 ± 6.2 19.7 ± 0.9*	0.14 ± 0.04 0.32 ± 0.01*	9.79 ± 5.08 16.24 ± 0.64*	0.14 ± 0.003
2k	Me	4-F-Ph-	24.5 ± 12.7	0.14 ± 0.04	5.71 ± 3.38	
2c	Me	3-Cl-Ph-	227.3 ± 120.5	0.16 ± 0.05	0.7 ± 0.43	
2h	Me	4-MeO-Ph-	1203.6 ± 118.7	0.24 ± 0.01	0.2 ± 0.02	
2i	Me	3-MeO-Ph-	622 ± 234.5	0.18 ± 0.05	0.29 ± 0.14	
2l	Me	4-CF_3-Ph-	*756.5 ± 251.7***	*0.05 ± 0.01***	*0.07 ± 0.03***	
2s	Me	1-naphthyl-	*15.6 ± 17.6***	*0.03 ± 0.002***	*1.92 ± 2.17***	
2u	Me	2,6-Cl-Ph	4118 ± 1204	0.23 ± 0.063	0.06 ± 0.02	
3a	*i*-Pr	Ph-	185.8 ± 115.1	0.16 ± 0.07	0.86 ± 0.65	
16	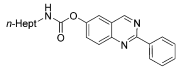		*1057.9 ± 577.7***	*0.14 ± 0.06***	*0.13 ± 0.09***	
physostigmine			280.3 ± 130.0	0.3 ± 0.1	0.3 ± 0.1	0.25 ± 0.01

[a]Asterisks indicate the following: (*) Values are measured for human BChE. (**) Values are calculated under the assumption of a pseudo-irreversible inhibition; they have to be carefully rated, as the inhibition mode might be different from that of the other inhibitors.

release of the carbamate C′ with k_4 as the decarbamoylation rate constant. Normally, k_4 is significantly lower than k_3 due to the fact that carbamoylation occurs much faster than decarbamoylation because of the high stability of E−C toward hydrolysis.

The values of K_C and k_3 can be quantified applying the method described by Hosie et al.[62] and Feaster et al.[63] Following this approach, the carbamate-mediated inhibition described in Figure 3 is known to undergo apparent first order kinetics:

$$A = A_0\, e^{-k_{obs}t} + A_\infty \quad (1)$$

in which A is the activity of the enzyme at a specific time t, A_0 the activity at $t = 0$, A_∞ the activity at $t = \infty$ and k_{obs} represents the apparent first order rate constant. Plotting of k_{obs} against the inhibitor concentration [PC] yields a hyperbolic curve described by

$$k_{obs} = \frac{k_3[PC]}{K_C\left(1 + \frac{[S]}{K_M}\right) + [PC]} \quad (2)$$

Rearrangement of eq 2 into a double reciprocal form with $1/k_{obs}$ as a function of $1/[PC]$ results in a linear plot:

$$\frac{1}{k_{obs}} = \frac{K_C\left(1 + \frac{[S]}{K_M}\right)}{k_3}\frac{1}{[PC]} + \frac{1}{k_3} \quad (3)$$

in which k_3 can be determined from the y-intercept and K_C from the slope. From these data also the second order rate constant k_3/K_C can be calculated describing the overall carbamoylation efficacy to evaluate differences in inhibitory potency. For the case, that substrate is not added from the beginning of the preincubation between inhibitor and enzyme, [S] becomes equal to zero because substrate and inhibitor are not competing for the binding pocket, and the substrate only adopts a function as reporter for remaining enzyme activity. In this case, eq 3 is simplified to

$$\frac{1}{k_{obs}} = \frac{K_C}{k_3}\frac{1}{[PC]} + \frac{1}{k_3} \quad (4)$$

On the basis of this method, we investigated kinetic parameters (Table 2) of a selected set of compounds including the reference compound **2a** and the highly potent inhibitors **2p** and **2k** as well as those compounds that showed differences in the Hill slopes of their IC_{50} curves compared to the other inhibitors (**2l**, **2s**, and **16**). The alkaloid physostigmine served as the external reference compound. In this series the thiophene compound **2p** was found as the most affine inhibitor with K_C = 14.3 nM and the one with the highest carbamoylation efficacy (k_3/K_C = 9.79 μM^{-1} min^{-1}). The fluorine substituted compound **2k** showed a comparably high affinity and carbamoylation efficacy. Interestingly, the twisted 2,6-dichloro compound **2u** displayed the lowest affinity to the enzyme with K_C = 4118 nM. This finding supports the hypothesis that a twist of the aromatic residue leads to decreased affinity toward the binding pocket (for details see Computational Studies). But even with this twist the carbamate is transferred to the serine. The only major exception for IC_{50} and K_C correlation was measured for the 1-naphthyl compound **2s** which showed a high affinity to the enzyme with K_C = 15.6 nM but an IC_{50} value in the micromolar range. Similar to the curves for determination of IC_{50} values, the shape of the obtained time-dependent inhibition curves was much less steep for compounds **2l**, **2s**, and **16** compared to all other inhibitors, indicating a different binding interaction.

For all compounds high carbamoylation rate constants k_3 were observed with similar values between 0.13 and 0.24 min^{-1}; exceptions were, as mentioned, the 1-naphthyl substituted derivative **2s** and also the 4-CF_3 analog **2l**. Apart from the exceptions, it can be assumed that similar values for k_3 have their origin in a similar orientation of the carbamate moiety with respect to the serine of the CAS, supporting a conserved binding mode of these inhibitors (see Computational Studies).

Enzyme recovery was measured exemplarily for the reference compound **2a** and the thiophenyl analog **2p**. For this purpose,

DOI: 10.1021/acs.jmedchem.5b01674
J. Med. Chem. XXXX, XXX, XXX−XXX

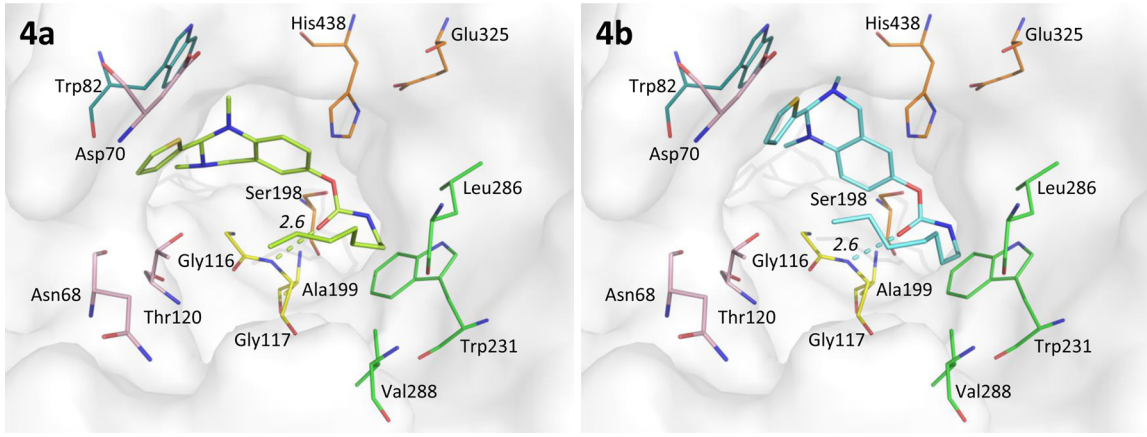

Figure 4. (a) Representation of the preferred binding mode for **2p** as *R*-enantiomer (light green) and (b) *S*-enantiomer (light blue) in the BChE binding site. Residues of the acyl pocket are shown in green, the oxyanion hole is in yellow, the CAS is in orange, the choline binding site (Trp82) is in turquoise, and parts of the side cavity are in pink. Distances in Å are given in italics. The figure was created with Pymol.[72]

the derivatives were incubated for 1 h with the enzyme at a concentration where complete inhibition was achieved and then successively 1000-fold diluted to a concentration where no carbamoylation was observed anymore. The recovery of the enzyme through hydrolysis of the carbamate residue was monitored after certain time points after dilution, showing first order kinetics with k_4 = 0.14 h^{-1} or a half-life for the carbamoylated enzyme of approximately 5 h. This value is identical for both compounds, as in both cases an *n*-heptyl carbamate is cleaved from the serine.

Taken together, the kinetic parameters reveal that (a) most inhibitors follow a conserved inhibition mode indicated by a similar carbamoylation rate constant k_3 and (b) they are only differing in their affinity expressed as K_C. It was observed that the exceptions **2l**, **2s**, and **16** probably do not adhere to this conserved binding mode, as shown by significant differences in the slope of their IC_{50} curves and kinetic parameters. Therefore, the results for these three inhibitors should be carefully rated, as the kinetic parameters were determined under the assumption of a pseudo-irreversible inhibition model, although the exact inhibition mode might in fact be different. These observations need to be further investigated.

We further investigated the most potent compound **2p** by performing enantiomeric resolution with HPLC on a chiral phase and chiropical analysis by CD spectroscopy. Although both enantiomers could be obtained after preparative chiral HPLC in their pure form (revealed by CD spectroscopy), they underwent rapid isomerization back into the racemic mixture (conditions and chromatograms are provided in the Supporting Information). It seems that racemization at the chiral center occurs by opening of the ring system into an imine structure which in turn reacts nonstereoselectively back to the ring system, thereby producing the racemate. Even though resolution of enantiomers was achieved, it can be assumed that isomerization of pure enantiomers into the racemate will occur at least in aqueous media during the biological testing of the compound. Assuming that the postulated binding modes (see Computational Studies) are correct, conformational energies and intermolecular scores of the respective binding poses suggest that in general the *S*-enantiomers might be more active than the *R*-enantiomers (see Supporting Information for further details).

We also investigated the kinetic properties of **2p** on human BChE (Table 2). We found this compound to have similar inhibitory activity on *h*BChE (as reported above for the IC_{50} values) compared to *eq*BChE with slightly decreased affinity (K_c = 19.7 nM), a higher carbamoylation rate (k_3 = 0.32 min^{-1}), and a higher carbamoylation efficacy (k_3/K_C = 16.24 μM^{-1} min^{-1}). With regard to the high similarity in inhibition and kinetic values of **2p** on *h*BChE and *eq*BChE, it can be assumed that all compounds synthesized will bind on *h*BChE and *eq*BChE in a similar manner.

Computational Studies. Modeling studies were performed in a combined docking and minimization approach with GOLD[64] and MiniMuDS.[65] For this purpose, the human BChE crystal structure 1P0I was used,[66] which possesses the highest resolution (2.0 Å) of BChE structures in the PDB.[67] Docking studies of reversible ligands of BChE had also been carried out by other groups.[43,68−70]

As the inhibitors were tested as racemic mixtures in the assay, both enantiomeric forms were built up and used for docking. All ligands of the series examined by detailed kinetic measurements (Table 2) as well as ligand **1** were used for docking studies.

For pseudo-irreversible inhibition, three different states may be addressed with classical docking methods: (1) A covalent docking can be carried out representing the carbamoylated serine (corresponding to E−C in Figure 3). As the carbamate stays the same throughout the data set, this approach was not performed here. (2) The tetrahedral transition state that occurs during the carbamoylation can be docked covalently to the serine. This method had been chosen by Carolan et al.[43] However, in this case a generally applicable interpretation for a set of compounds in light of the inhibition and kinetic data was not possible. Therefore, (3) the inhibitor structures were docked non-covalently to BChE to mimic reversible inhibition by formation of the initial noncovalent complex ((EPC) in Figure 3). These docking data can be analyzed in relation to the experimentally determined K_C values.

Docking poses of inhibitor **1** showed the same binding mode for both enantiomeric forms on the top (*S*-enantiomer) and the second-best rank (*R*-enantiomer) (see Experimental Section for a detailed description of pose selection). These poses were taken as reference poses to model the binding mode of the other inhibitor structures by deletion and addition of the corresponding functional groups and subsequent local minimization in the binding site using MiniMuDS. The methyl group on the benzylic nitrogen can adopt a pseudo-equatorial or pseudo-axial

DOI: 10.1021/acs.jmedchem.5b01674
J. Med. Chem. XXXX, XXX, XXX−XXX

orientation. The herein displayed structures show the methyl group in the pseudo-equatorial position for the *R*-enantiomer and in the pseudo-axial position for the *S*-enantiomer, as these orientations were found to be preferred.

The binding mode of the compounds is characterized by the following features: The *n*-heptyl chain is placed over the acyl binding site (mainly formed by Trp231, Leu286, and Val288). The carbamate moiety is positioned near His438 and Ser198 (together with Glu325 the CAS comprising amino acids), showing distances of the carbamate carbon to the serine oxygen of 2.9−3.0 Å and 3.6−4.1 Å for the *R*- and *S*-enantiomers, respectively. The oxygen of the carbamate moiety is oriented toward Gly117-NH in hydrogen bond distances of 2.6−2.9 Å and 2.6−3.0 Å for the *R*- and *S*-enantiomers, respectively. Gly116, Gly117, and Ala119 form the oxyanion hole. These residues are important in stabilizing the negative charge formed at the carbonyl oxygen during substrate hydrolysis.[71]

The tetrahydroquinazoline is placed "above" the oxyanion hole, and the aromatic ring is in $\pi-\pi$ interaction distances of 3.4 and 3.8 Å to His438 (measured for *S*- and *R*-**2p**, respectively). The aryl rings (the substituents R^2 of Table 2) are placed in a cavity "below" Trp82, formed by Asn68, Asp70, and Thr120 (colored in pink in Figure 4).

The ligand poses derived from ligand **1** show the aryl ring "in plane" with the tetrahydroquinazoline (more precisely, the bond between the aryl ring and the tetrahydroquinazoline shows a dihedral angle of approximately 0°). However, a twisted conformation with a ∼90° dihedral, similar as in ortho-substituted biaryls,[73] would also be possible. To test whether the "in plane" or "twisted" orientation of the aryl ring is favored, compound **2u**, a 2,6-dichloro derivative, was therefore synthesized. Due to steric hindrance of the ortho-chloro substituents and the methyl groups on the quinazoline core, the aryl ring needs to adopt the twisted conformation. As the affinity of this compound (K_C = 4118 nM) is the lowest in the tested series, the twisted conformation is apparently not favorable for high-affinity binders. As the modeled ligand pose shows, without a displacement from the generally preferred binding mode, this conformation would lead to clashes with the protein. Thus, except for **2u**, the aryl ring can be assumed to be "in plane" with the tetrahydroquinazoline core as shown in Figure 4.

Although a quantitative correlation between the docking scores and the activity of the compounds cannot be expected (primarily due to the well-known accuracy limitations of scoring functions and the uncertain contribution of the enantiomers to the experimentally measured affinities of the racemic compounds), some differences in affinity (in terms of K_C) can qualitatively be explained by the structural differences of the inhibitors in this binding model. Compared to the thiophene derivative **2p** as the smallest compound, the significantly weaker affinity of compounds with sterically demanding para-substituents (**2h**, **2l**) is in line with the steric restrictions imposed by the side cavity (formed by Ile69, Asn83, and Pro84) to which these para-substituents point. Especially the para-CF_3 compound **2l** leads to clashes with the protein when forcing it into a similar binding mode as identified for thiophene derivative **2p** (see Figure S5 in the Supporting Information). This is in agreement with the different kinetic profile and supports the hypothesis of a different binding mode for this compound. Although not forming particularly favorable interactions, meta-substituents (cf. **2c**, **2i**) are better tolerated because they point "upward" to a more accessible area. Additional interactions in this region can be formed by the 1-naphthyl group (**2s**), which might overall lead to the similarly favorable affinity as observed for **2p**. However, because of the different kinetic characteristics described above, caution is warranted in interpreting the results for compound **2s** (as well as for **2l**). This also applies to the achiral compound **16**, which served as a test compound to confirm the binding mode without the uncertainty of enantiomeric forms. However, docking showed that the planar shape of the ligand cannot be accommodated in the common binding mode adopted by the other inhibitors. This could indicate a different mode of action, as suggested also by the kinetic data.

Antioxidant Capacity, Neuroprotection, and Neurotoxicity. Neuronal cell death induced by reactive oxygen species (ROS) is prevented by antioxidants that contain radical scavenging structures. The determination of these antioxidant capacities can be achieved by the oxygen radical absorbance capacity (ORAC) assay in which the ability of an antioxidant to reduce the amount of induced peroxylradicals is determined. This test therefore describes direct physiochemical radical scavenging properties of compounds but does not necessarily directly relate to results from cell-based methods,[36,47] although often claimed in the literature. Results in this assay are expressed in relation to the radical scavenging properties of 6-hydroxy-2,5,7,8-tetramethylchroman-2-carboxylic acid (also called Trolox, a water-soluble vitamin E analog) yielding the Trolox equivalents (TE) unit.

In this work, the synthesized carbamates release the corresponding carrier phenols after carbamate transfer onto BChE (compare Figure 2b),[36,47] which can act as potent radical scavengers with their *p*-aminohydroquinone moiety. Therefore, we chose pairs of compounds (carbamates and corresponding phenols) to investigate and correlate their antioxdative properties, including the unsubstituted compound **2a**, the thiophene bearing compound **2p** as a highly potent BChE inhibitor, the 4-MeO bearing compound **2h** as a relatively weak BChE inhibitors, and the *N*-benzyl containing compound **3c** as well as their phenolic analogs **9a**,**p**,**h** and **10c**. The results for the ORAC assay are summarized in Table 3. All of the tested carbamates show by

Table 3. Antioxidant Capacities of Target Compounds Expressed as Trolox Equivalents (TE)

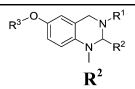

R^1	R^2	R^3 = H		R^3 = *n*-Hept-NHC(O)-	
Me	Ph	**9a**	3.0 ± 0.3	**2a**	0.2 ± 0.1
Me	2-thiophenyl-	**9p**	3.4 ± 0.1	**2p**	0.2 ± 0.1
Me	4-MeO-Ph-	**9h**	3.7 ± 0.3	**2h**	0.5 ± 0.2
Bn	Ph	**10c**	3.9 ± 0.4	**3c**	1.7 ± 0.2

themselves radical scavenging properties with antioxidant capacities between 0.2 and 0.5 TE. A remarkable difference can be observed for the *N*-benzyl bearing compound **3c** with an antioxidant capacity of 1.7 which might be explained by the possibility to form stable benzyl radicals, thereby acting as a strong antioxidant exceeding Trolox already in its carbamate form.

As expected, the antioxidant capacities of the hydroxy compounds **9** and **10** were significantly higher than those of their corresponding carbamates and of the positive control and reference Trolox, itself ranging from 3.0 to 3.9 TE. The *N*-benzyl bearing tetrahydroquinazoline **10c** shows the highest antioxidant capacity with 3.9 TE in this series, as it might be able to trap radicals with its *p*-aminohydroquinone core and additionally with

DOI: 10.1021/acs.jmedchem.5b01674
J. Med. Chem. XXXX, XXX, XXX−XXX

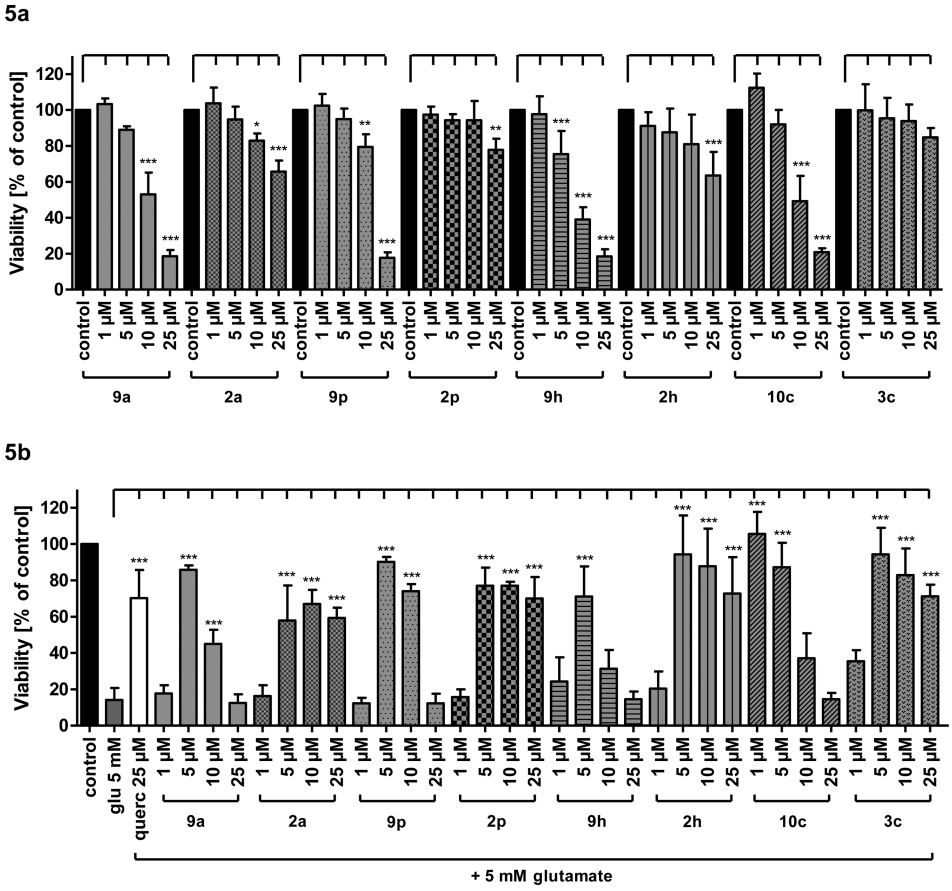

Figure 5. (a) Neurotoxicity tests for target compounds on HT-22 cells. (b) Neuroprotection tests against glutamate induced oxidative stress for target compounds on HT-22 cells.

the benzyl group as mentioned before for the carbamate **10c**. In summary, it was observed that the carbamates by themselves show already antioxidant capacities, albeit only moderate ones, and their corresponding phenols released after carbamate transfer onto the active site of BChE represent highly potent radical scavengers with 3- to 4-fold higher antioxidant capacities than Trolox.

As mentioned above, evaluation of compounds in a cellular neuronal assay provides additional information with respect to therapeutic applications, since it enables assessment of how well physicochemical properties translate into biological settings. In fact correlating both methods is most meaningful. Therefore, to evaluate the ability of the target compounds to prevent oxycytotic cell death after glutamate exposure, the compounds were applied onto a model system with the glutamate sensitive murine hippocampal HT-22 cells which lack an ionotropic glutamate receptor. These cells contain a glutamate−cysteine antiporter that is necessary for the cysteine uptake from the extracellular side under physiological conditions and at the same time transports glutamate out of the cytosol.[74] When HT-22 cells are exposed to high glutamate concentrations, this transporter is blocked by extracellular glutamate. In consequence, no cysteine is uptaken for glutathione (GSH) synthesis, the antioxidant protecting from intracellular ROS induced cell death.[75−77]

The same compounds evaluated in the ORAC assay were tested for neuroprotection on HT-22 cell line with the natural product quercetin as the antioxidant reference. Cells were incubated with the compounds in different concentrations either with 5 mM glutamate to induce oxycytosis or without glutamate to determine self-toxicity toward the cells (Figure 5). In general, all tested hydroxy compounds (series **9** and **10**) showed similar effects on HT-22 cells with no or only little toxicity at concentrations of 1 and 5 μM (Figure 5a). The carbamates (series **2** and **3**) are even less neurotoxic compared to the corresponding phenols. The cell viability was maintained above 80% for all carbamates up to a concentration of 10 μM. Interestingly the *N*-benzyl carbamate **3c** showed no significant decrease in cell viability even at the highest concentration of 25 μM.

When glutamate was added to induce oxidative stress (Figure 5b), the phenols very effectively counteracted glutamate-induced neurotoxicity already at a concentration of 5 μM as the cell viability was maintained. Decreasing viability at higher concentrations relates to neurotoxic effects for compounds like **9h** and **10c** but is only significant at 25 μM. Furthermore, the *N*-benzyl containing phenol **10c** maintained cell viability at already 1 μM, proving its high neuroprotectivity already at low concentrations.

It is remarkable that also the carbamate-based structures (series **2** and **3**) showed at concentrations above 5 μM that cell viability is comparable to the one of the reference compound quercetin at 25 μM, proving their neuroprotective effect. This finding is quite of interest, since hydrolysis to the phenol is not necessary for cell-based neuroprotective effects.

However, neuroprotection assays suffer from the drawback that the concentrations needed to be applied in such assays are much higher than what is expected for a ligand/inhibitor to be effective in vivo. This is because respective assays are not

DOI: 10.1021/acs.jmedchem.5b01674
J. Med. Chem. XXXX, XXX, XXX−XXX

sensitive enough and the data therefore have to be correlated to the positive control (in our case Trolox in the ORAC assay and quercetin in the HT-22 assay). Compared to quercetin (applied at 25 μM) the compounds are more active even at lower concentrations than for quercetin.

In summary, the compounds described are not only very potent and selective BChE inhibitors but also act as highly active neuroprotectants both by themselves and after release of the phenolic carrier.

CONCLUSION

In this report we identified a set of pseudo-irreversible carbamate-based inhibitors of BChE (**2a−u**, **3a−c**, and **16**) by applying rational approaches to conduct SARs of the tetrahydroquinazoline carrier scaffold. Although the corresponding phenolic tetrahydroquinazolines **9a−u**, **10a−c**, and **15** showed BChE inhibition in the micromolar range lacking significant selectivity over *h*AChE, they are the source of the modulated affinity of the carbamate series. In this series we found thiophene compound **2p** as the most potent inhibitor with regard to both affinity (K_C = 14.3 nM) and carbamoylation efficacy (k_3/K_C = 9.79 μM^{-1} min^{-1}) toward the enzyme. To our knowledge, this compound represents by far one of the most active and selective inhibitors of BChE described to date.

By combining kinetic investigations with computational studies, we established a model for binding of the tetrahydroquinazoline scaffold and therefore for modulated affinity of the inhibitors toward the enzyme. In the computational studies, the heterocyclic inhibitors place their carbamate moieties in close proximity to the serine of the CAS. This accounts for appropriate preorientation for the subsequent transfer of the carbamate. Substituents on the aryl ring that are responsible for affinity of this set of compounds bind to a side cavity of BChE's active site located next to the entrance of the binding site. Both kinetic data and computational studies support a conserved binding mode for the described inhibitors, with the exception of the 4-CF_3-substituted compounds **2l**, 1-naphthyl compound **2s**, and the planar quinazoline **16**. Combining computational studies with kinetic values can be considered as a general approach to investigate the binding mode of carbamate-based pseudo-irreversible inhibitors, as the binding mode of these inhibitors is similar.

Neuroprotective abilities for a subset of carbamates and their corresponding phenols were determined in an ORAC assay and a neuronal cell-based one and revealed high radical scavenging properties of the phenolic heterocycle carrier scaffold formed after transfer of the carbamate moiety to the enzyme. Pronounced neuroprotection comparable to quercetin was seen when intracellular oxidative stress was triggered through glutamate exposure in neuronal cells.

In addition to the development of improved and neuroprotective BChE inhibitors, our results might be of relevance for a general methodology to be applied for development of other pseudo-irreversible enzyme inhibitors.

EXPERIMENTAL SECTION

Chemistry. General. Common reagents and solvents were obtained from commercial suppliers and used without any further purification. Tetrahydrofuran (THF) was distilled from sodium/benzophenone under argon atmosphere. Reaction progress was monitored using analytical thin layer chromatography (TLC) on precoated silica gel GF_{254} plates (Macherey-Nagel GmbH & Co. KG, Düren, Germany), and spots were detected under UV light (254 nm) or through staining with iodine. Nuclear magnetic resonance spectra were performed with a Bruker AV-400 NMR instrument (Bruker, Karlsruhe, Germany) in DMSO-d_6 or $CDCl_3$. Chemical shifts are expressed in ppm relative to $CDCl_3$ or DMSO-d_6 (7.26/2.50 and 77.16/39.52 ppm for ^1H and ^{13}C NMR, respectively). Melting points were determined in open capillaries on a Büchi B-540 without any further correction except for the phenolic tetrahydroquinazolines, as they undergo rapid decomposition during heating. For purity of target compounds, analytic HPLC was performed on a system from Shimadzu equipped with a DGU-20A3R controller, LC20AB liquid chromatograph, and a SPD-20A UV/vis detector. Stationary phase was a Synergi 4U fusion-RP (150 mm × 4.6 mm) column (Phenomenex, Aschaffenburg, Germany). As mobile phase, water (phase A) and MeOH (phase B) were used with 1 mL/min. (Method A: conc B, 5% → 90% from 0 to 8 min; 90% from 8 to 13 min; 90% → 5% from 13 to 15 min; 5% from 15 to 18 min. Method B: conc B, 10% → 80% from 0 to 8 min; 80% from 8 to 13 min; 80% → 10% from 13 to 15 min; 10% from 15 to 18 min. Method C: conc B, 30% → 90% from 0 to 8 min; 90% from 8 to 13 min; 90% → 30% from 13 to 15 min; 30% from 15 to 18 min) Target compounds were ≥95% pure. Purities of **9r** and **10a** were determined by CHN analysis on a Vario MICRO CUBE (Elementar Analysesysteme GmbH, Hanau, Germany) because of their low stability on HPLC. ESI mass spectral data were acquired on a Simadzu LCMS-2020.

General Reactions. General Amide Formation Procedure (GP1). 6-Hydroxy-1-methyl-2*H*-benzo[*d*][1,3]oxazine-2,4(1*H*)-dione **5** was dissolved in dry DMF (30 mL) and treated with the corresponding amine (5 equiv) or a mixture of the amine hydrochloride (5 equiv) and triethylamine (5 equiv). The mixture was heated to 40−120 °C (depending on the amine) for 4−5 h. For workup, the mixture was poured into water (100 mL) and the product was extracted with ethyl acetate (5 × 100 mL). The combined organic layers were washed with brine (50 mL), dried over Na_2SO_4, and evaporated to dryness. The crude product was purified by column chromatography to obtain 5-hydroxy-*N*-methyl-2-(alkylamino)benzamides **6a−d**.

General Cyclization Procedure (GP2). 5-Hydroxy-*N*-methyl-2-(alkylamino)benzamides **6a−d** were dissolved in glacial acetic acid (20 mL). The mixture was treated with the corresponding aldehyde (1.2 equiv) and heated to 70 °C for 1−3 h. Then the mixture was poured onto ice−water (20 mL), basified with a NaOH solution (2 M) and the pH was adjusted to 9 with sat. NH_4Cl solution. The product was extracted with ethyl acetate (3 × 40 mL), the combined organic layers were washed with brine (30 mL), dried over Na_2SO_4, and the solvent was evaporated under reduced pressure. The crude product was either recrystallized or purified by column chromatography to obtain dihydroquinazolinones **7a−u** and **8a−c**.

General Reduction Procedure (GP3). Dihydroquinazolinones **7a−u** and **8a−c** were dissolved in dry THF (30 mL) at 0 °C, and $LiAlH_4$ (4 equiv) was added. The mixture was allowed to reach rt and was then heated to reflux temperature for 1−3 h. After cooling to rt, the mixture was poured into ice−water (50 mL) followed by the addition of saturated NH_4Cl solution until pH = 9. The aqueous phase was then extracted with ethyl acetate (3 × 80 mL). The combined organic layers were washed with brine (50 mL), dried over Na_2SO_4, and the solvent was evaporated under reduced pressure. The crude product was purified by column chromatography to obtain the corresponding tetrahydroquinazolines **9a−u** and **10a−c**.

General Carbamate Formation Procedure (GP4). A solution of tetrahydroquinazolines **9a−n**, **9q−u**, and **10a−c** in dry THF (5 mL) was treated with NaH in paraffin oil (60%, 1.2 equiv). The mixture was stirred until the formation of gas stopped. Then, a solution of 4-nitrophenyl-*n*-heptylcarbamate (1.2 equiv) in dry THF (3 mL) was added at once. The mixture was stirred for 2 h. For workup, the mixture was diluted with ethyl acetate (30 mL), washed with water (10 mL), and washed with brine (10 mL). The organic phase was dried over Na_2SO_4, and the solvent was evaporated under reduced pressure. The crude product was purified by column chromatography to obtain the corresponding *n*-heptylcarbamate **2a−n**, **2q−u**, and **3a−c**.

Synthesis and Spectral Data. Syntheses of **4** and **5** were performed as described.[49] The synthesis of target compound **2a** is

DOI: 10.1021/acs.jmedchem.5b01674
J. Med. Chem. XXXX, XXX, XXX−XXX

exemplarily given in the following. For synthetic procedures and spectral data of **2b−u** and **3a−c** see Supporting Information.

5-Hydroxy-*N*-methyl-2-(methylamino)benzamide 6a. According to GP1, 6-hydroxy-1-methyl-1*H*-benzo[*d*][1,3]oxazine-2,4-dione **5** (500 mg, 2.59 mmol, 1 equiv), methylamine hydrochloride (874 mg, 12.95 mmol, 5 equiv), and triethylamine (1.79 mL, 12.95 mmol, 5 equiv) were used to obtain 5-hydroxy-*N*-methyl-2-(methylamino)benzamide **6a** (321 mg, 69%) after column chromatography (petroleum ether/EtOAc = 1:4) as a yellow-brown solid; mp 164−166 °C. ^{1}H NMR (400 MHz, DMSO-d_6): δ = 8.59 (s, OH), 8.15 (q, J = 4.2 Hz, NH), 6.92 (d, J = 2.8 Hz, 1H), 6.85 (q, J = 4.3 Hz, NH), 6.80 (dd, J = 8.8, 2.8 Hz, 1H), 6.49 (d, J = 8.8 Hz, 1H), 2.71 (d, J = 1.3 Hz, 3H), 2.70 (d, J = 2.0 Hz, 3H) ppm. ^{13}C NMR (101 MHz, DMSO-d_6): δ = 169.4, 146.5, 143.3, 119.6, 116.7, 114.6, 111.6, 30.0, 26.0 ppm. ESI-MS: m/z calcd, 180.09; found, 181.2 $[M + H]^+$.

6-Hydroxy-1,3-dimethyl-2-phenyl-2,3-dihydroquinazolin-4(1*H*)-one 7a. According to GP2, 5-hydroxy-*N*-methyl-2-(methylamino)benzamide **6a** (170 mg, 0.94 mmol, 1 equiv) and benzaldehyde (114 μL, 1.13 mmol, 1.2 equiv) were used to obtain 6-hydroxy-1,3-dimethyl-2-phenyl-2,3-dihydroquinazolin-4(1*H*)-one **7a** (167 mg, 66%) after column chromatography (petroleum ether/EtOAc = 1:2) as a yellow solid; mp 205−207 °C. ^{1}H NMR (400 MHz, DMSO-d_6): δ = 8.99 (s, OH), 7.35−7.27 (m, 3H), 7.22 (d, J = 2.9 Hz, 1H), 7.19−7.09 (m, 2H), 6.80 (dd, J = 8.7, 3.0 Hz, 1H), 6.46 (d, J = 8.7 Hz, 1H), 5.67 (s, 1H), 2.90 (s, 3H), 2.73 (s, 3H) ppm. ^{13}C NMR (101 MHz, DMSO-d_6): δ = 161.7, 149.6, 139.4, 136.8, 128.6, 128.5 (2C), 126.2 (2C), 120.9, 117.6, 114.1, 113.4, 78.6, 35.7, 32.1 ppm. ESI-MS: m/z calcd, 268.12; found, 559.25 $[2M + Na]^+$.

1,3-Dimethyl-2-phenyl-1,2,3,4-tetrahydroquinazolin-6-ol 9a. According to GP3, starting from 6-hydroxy-1,3-dimethyl-2-phenyl-2,3-dihydroquinazolin-4(1*H*)-one **7a** (160 mg, 0.6 mmol, 1 equiv) the title compound 1,3-dimethyl-2-phenyl-1,2,3,4-tetrahydroquinazolin-6-ol **9a** (79 mg, 52%) was obtained as a pale yellow solid. ^{1}H NMR (400 MHz, DMSO-d_6): δ = 8.42 (s, OH), 7.34−7.27 (m, 2H), 7.27−7.21 (m, 1H), 7.18−7.08 (m, 2H), 6.56 (dd, J = 8.6, 2.7 Hz, 1H), 6.51 (d, J = 8.7 Hz, 1H), 6.32 (d, J = 2.6 Hz, 1H), 4.83 (s, 1H), 3.50 (d, J = 16.2 Hz, 1H), 3.27 (d, J = 16.1 Hz, 1H), 2.84 (s, 3H), 2.36 (s, 3H) ppm. ^{13}C NMR (101 MHz, DMSO-d_6): δ = 147.8, 141.1, 136.7, 128.1 (2C), 127.3, 126.9 (2C), 119.1, 114.1, 113.9, 110.1, 80.7, 49.2, 41.6, 36.8 ppm. ESI-MS: m/z calcd, 254.14; found, 255.2 $[M + H]^+$. HPLC (method A): 98%.

1,3-Dimethyl-2-phenyl-1,2,3,4-tetrahydroquinazolin-6-yl *n*-Heptylcarbamate 2a. According to GP4, starting from 1,3-dimethyl-2-phenyl-1,2,3,4-tetrahydroquinazolin-6-ol **9a** (120 mg, 0.47 mmol, 1 equiv) the title compound 1,3-dimethyl-2-phenyl-1,2,3,4-tetrahydroquinazolin-6-yl *n*-heptylcarbamate **2a** (95 mg, 51%) was obtained after column chromatography (DCM/MeOH = 95:5) as white solid; mp 93−95 °C. ^{1}H NMR (400 MHz, DMSO-d_6): δ = 7.51 (t, J = 5.7 Hz, NH), 7.36−7.29 (m, 2H), 7.29−7.23 (m, 1H), 7.15 (d, J = 7.1 Hz, 2H), 6.82 (dd, J = 8.7, 2.7 Hz, 1H), 6.62 (d, J = 8.9 Hz, 1H), 6.60 (d, J = 2.7 Hz, 1H), 4.96 (s, 1H), 3.56−3.49 (m, 1H), 3.36−3.30 (m, 1H), 3.01 (dd, J = 13.0, 6.7 Hz, 2H), 2.92 (s, 3H), 2.40 (s, 3H), 1.50−1.38 (m, 2H), 1.27 (s, 8H), 0.87 (t, J = 6.8 Hz, 3H) ppm. ^{13}C NMR (101 MHz, DMSO-d_6): δ = 155.1, 141.0, 140.9, 140.6, 128.2 (2C), 127.5, 126.7 (2C), 120.6, 120.1, 118.0, 108.8, 80.5, 48.5, 41.6, 40.4, 36.7, 31.2, 29.2, 28.4, 26.2, 22.0, 13.9 ppm. ESI-MS: m/z calcd, 395.26; found, 396.3 $[M + H]^+$. HPLC (method B): 100%.

5-(Benzyloxy)-2-nitrobenzaldehyde 11. A solution of 5-hydroxy-2-nitrobenzaldehyde (2 g, 11.98 mmol, 1 equiv) in dry DMF (40 mL) was treated with benzyl bromide (2.85 mL, 23.95 mmol, 2 equiv) and potassium carbonate (3.3 g, 23.95 mmol, 2 equiv). The reaction mixture was stirred for 48 h at 40 °C. Then ice cold water (100 mL) was added and the mixture was stirred for further 15 min. The precipitated solid was filtered and washed with petroleum ether (20 mL) to obtain 5-(benzyloxy)-2-nitrobenzaldehyde **11** (2.86 g, 88%) as a yellow solid; mp 68−70 °C. ^{1}H NMR (400 MHz, $CDCl_3$): δ = 10.48 (s, 1H), 8.16 (d, J = 9.1 Hz, 1H), 7.46−7.30 (m, 6H), 7.21 (dd, J = 9.1, 2.9 Hz, 1H), 5.20 (s, 2H) ppm. ^{13}C NMR (101 MHz, $CDCl_3$): δ = 188.4, 163.1, 142. 5, 135.0, 134.3, 128.9 (2C), 128.7, 127.6 (2C), 127.3, 119.3, 114.2, 71.1 ppm.

2-Amino-5-(benzyloxy)benzaldehyde 12. 5-(Benzyloxy)-2-nitrobenzaldehyde **11** (2.83 g, 10.44 mmol, 1 equiv) was dissolved in EtOH/H_2O (4:1, 50 mL) and treated with elementary iron (5.85 g, 104.4 mmol, 10 equiv) and a catalytic amount of conc HCl solution (50 μL). The mixture was heated to reflux temperature for 1 h. The product was then extracted with ethyl acetate (3 × 100 mL), and the combined organic layers were washed with brine (50 mL) and dried over Na_2SO_4. After removal of the solvent under reduced pressure, 2-amino-5-(benzyloxy)benzaldehyde **12** (1.44 g, 61%) was obtained as a yellow solid; mp 83 °C. ^{1}H NMR (400 MHz, $CDCl_3$): δ = 9.74 (d, J = 0.5 Hz, 1H), 7.38−7.21 (m, 5H), 6.99 (dd, J = 8.7, 2.9 Hz, 1H), 6.96 (d, J = 2.8 Hz, 1H), 6.54 (d, J = 8.7 Hz, 1H), 5.77 (s, NH_2), 4.95 (s, 2H) ppm. ^{13}C NMR (101 MHz, $CDCl_3$): δ = 193.5, 149.9, 145.0, 137.0, 128.6 (2C), 128.1, 127.5 (2C), 125.5, 118.7, 118.5, 117.6, 71.1 ppm. ESI-MS: m/z calcd, 227.09; found, 228.10 $[M + H]^+$.

***N*-(4-(Benzyloxy)-2-formylphenyl)benzamide 13.** A mixture of 2-amino-5-(benzyloxy)benzaldehyde **12** (1022 mg, 4.49 mmol, 1 equiv) and triethylamine (934 μL, 4.63 mmol, 1.2 equiv) was dissolved in DCM (50 mL) and treated dropwise with benzoyl chloride (784 μL, 6.75 mmol, 1.5 equiv). After stirring for 4 h, the reaction mixture was diluted with DCM (100 mL) and washed with 2 M HCl (50 mL), sat. $NaHCO_3$ (50 mL), and brine (50 mL). The solvent was removed under reduced pressure and the crude product was purified by column chromatography (DCM/petroleum ether = 1:1) to obtain *N*-(4-(benzyloxy)-2-formylphenyl)benzamide **13** (986 mg, 66%) as a yellow solid; mp 131−133 °C. ^{1}H NMR (400 MHz, $CDCl_3$): δ = 11.84 (s, NH), 9.94 (d, J = 0.6 Hz, 1H), 8.92 (d, J = 9.1 Hz, 1H), 8.12−8.03 (m, 2H), 7.60−7.50 (m, 3H), 7.48−7.38 (m, 4H), 7.38−7.34 (m, 1H), 7.32 (dd, J = 9.0, 3.0 Hz, 1H), 7.29 (d, J = 2.9 Hz, 1H), 5.14 (s, 2H) ppm. ^{13}C NMR (101 MHz, $CDCl_3$): δ = 195.5, 165.8, 154.3, 136.3, 135.2, 134.5, 132.0, 128.9 (2C), 128.7 (2C), 128.3, 127.5 (2C), 127.4 (2C), 123.3, 122.9, 121.8, 121.1, 70.7 ppm. ESI-MS: m/z calcd, 331.12; found, 332.15 $[M + H]^+$.

6-(Benzyloxy)-2-phenylquinazoline 14. According to the literature,[50] *N*-(4-(benzyloxy)-2-formylphenyl)benzamide **13** (980 mg, 2.96 mmol, 1 equiv) was suspended in *i*-PrOH/conc ammonia (1:1, 30 mL) and heated to 90 °C for 6 h under microwave irradiation. Then the product was extracted with ethyl acetate (2 × 100 mL), the combined organic layers were washed with brine (50 mL) and dried over Na_2SO_4. After removal of the solvent, 6-(benzyloxy)-2-phenylquinazoline **14** (889 mg, 96%) was obtained as a beige solid; mp 119−120 °C. ^{1}H NMR (400 MHz, $CDCl_3$): δ = 9.38 (d, J = 0.7 Hz, 1H), 8.63−8.56 (m, 2H), 8.04 (d, J = 9.2 Hz, 1H), 7.66 (dd, J = 9.2, 2.8 Hz, 1H), 7.58−7.51 (m, 5H), 7.51−7.43 (m, 2H), 7.43−7.36 (m, 1H), 7.27 (d, J = 2.8 Hz, 1H), 5.25 (s, 2H) ppm. ^{13}C NMR (101 MHz, $CDCl_3$): δ = 159.6, 158.9, 157.3, 147.1, 138.2, 136.1, 130.3, 130.2, 128.8 (2C), 128.6 (2C), 128.4, 128.2 (2C), 127.6 (2C), 127.5, 124.5, 105.3, 70.6 ppm. ESI-MS: m/z calcd, 312.13; found, 313.20 $[M + H]^+$.

2-Phenylquinazolin-6-ol 15. 6-(Benzyloxy)-2-phenylquinazoline **14** (870 mg, 2.79 mmol, 1 equiv) was dissolved in MeOH (50 mL), and Pd/C (87 mg, 10 wt %) was added. The atmosphere of the reaction vessel was removed under reduced pressure, and then the vessel was purged with hydrogen. The mixture was heated to 50 °C for 3 h. Then the mixture was filtered over a short silica column to obtain 2-phenylquinazolin-6-ol **15** (435 mg, 70%) as a white solid; mp 233−235 °C. ^{1}H NMR (400 MHz, DMSO-d_6): δ = 10.44 (br, OH), 9.50 (d, J = 0.7 Hz, 1H), 8.58−8.43 (m, 2H), 7.95 (d, J = 9.1 Hz, 1H), 7.61−7.48 (m, 4H), 7.32 (d, J = 2.6 Hz, 1H) ppm. ^{13}C NMR (101 MHz, DMSO-d_6): δ = 159.7, 157.7, 156.9, 145.4, 138.3, 130.6, 130.1, 129.1 (2C), 128.1 (2C), 127.7, 125.2, 108.2 ppm. ESI-MS: m/z calcd, 222.08; found, 223.15 $[M + H]^+$. HPLC (method A): 100%.

2-Phenylquinazolin-6-yl *n*-Heptylcarbamate 16. According to GP4, starting from 2-phenylquinazolin-6-ol **15** (60 mg, 0.27 mmol, 1 equiv) the title compound 2-phenylquinazolin-6-yl heptylcarbamate **16** (35 mg, 36%) was obtained after column chromatography (petroleum ether/EtOAc = 3:1) as white powder; mp 141−144 °C. ^{1}H NMR (400 MHz, $CDCl_3$): δ = 9.41 (s, 1H), 8.64−8.55 (m, 2H), 8.07 (d, J = 9.1 Hz, 1H), 7.71 (d, J = 2.4 Hz, 1H), 7.66 (dd, J = 9.1, 2.6 Hz, 1H), 7.58−7.48 (m, 3H), 5.20 (t, J = 5.6 Hz, NH), 3.29 (dd, J = 13.3, 7.0 Hz, 2H), 1.67−1.49 (m, 2H), 1.44−1.23 (m, 8H), 0.90 (t, J = 6.9 Hz, 3H) ppm. ^{13}C NMR (101 MHz, $CDCl_3$): δ = 160.8, 160.0, 154.0, 149.3, 148.5, 137.9,

DOI: 10.1021/acs.jmedchem.5b01674
J. Med. Chem. XXXX, XXX, XXX−XXX

130.6, 130.0, 129.7, 128.6 (2C), 128.5 (2C), 123.7, 117.3, 41.4, 31.7, 29.8, 28.9, 26.7, 22.6, 14.1 ppm. ESI-MS: m/z calcd, 363.19; found, 364.25 $[M + H]^+$. HPLC (method B): 100%.

Enzyme Inhibition. AChE (EC 3.1.1.7, from human erythrocytes) and BChE (EC 3.1.1.8, from equine serum and from human serum) were purchased from Sigma-Aldrich (Steinheim, Germany). DTNB (Ellman's reagent), ATC and BTC iodides were obtained from Fluka (Buchs, Switzerland). The stock solutions of the test compounds were prepared in ethanol with a concentration of 33.3 mM (1 mM in assay) and stepwise diluted with ethanol to a concentration of 33.3 nM (1 nM in assay). For assay buffer preparation, an amount of 3.12 g of potassium dihydrogen phosphate was dissolved in 500 mL of water and adjusted with a NaOH solution (0.2 M) to pH = 8.0. Enzyme solutions were prepared with buffer to give 2.5 units/mL and stabilized with 2 mg of albumin bovine (SERVA, Heidelberg, Germany) per mL of enzyme solution. An amount of 396 mg of DTNB was dissolved in 100 mL of buffer to give a 10 mM solution (0.3 mM in assay). ATC and BTC solutions were prepared in buffer with a concentration of 75 mM (452 μM in assay). The assay was performed at 25 °C as described in the following: Into a cuvette containing 1.5 mL of buffer, 50 μL of the respective enzyme, and 50 μL of DTNB solution, the test compound solution (50 μL) was added, and the mixture was mixed. The mixture was incubated for 4.5 min (phenols) or 30 min (carbamates), before an amount of 10 μL of ATC or BTC (depending on the enzyme) was added. The mixture was incubated for further 2.5 min before the absorption at 412 nm was determined with a Shimadzu UVmini-1240 spectrophotometer. To measure full enzyme activity, the compound solution was replaced by ethanol. Each compound concentration was tested three times. The enzyme activity in percentage was plotted against the logarithm of the compound concentrations from which the IC_{50} values were calculated by the software GraphPad Prism 4.

Enzyme Kinetics. Carbamoylation kinetics were measured following the enzyme inhibition protocol. For this purpose, the enzyme was 5, 10, 20, 30, and 40 min preincubated with different inhibitor concentrations before the addition of substrate. Plotting the enzyme activity in percentage as a function of time for each inhibitor concentration gave nonlinear time dependent inhibition curves from which k_{obs} was determined by eq 1. Double reciprocal plot of $1/k_{obs}$ against $1/c$(inhibitor) gave a linear plot from which k_3 and K_C were determined by eq 4. Decarbamoylation kinetics were measured by incubating the enzyme with an inhibitor concentration that fully inhibits the enzyme for 1 h. This mixture was then diluted 1:1000 with assay buffer to prevent further enzyme inhibition. The assay was then performed as described in the enzyme inhibition protocol at different time points after the dilution to determine recovery of enzyme activity. Uninhibited enzyme was treated by the same procedure to access control values for enzyme activity after dilution. Plotting the enzyme activity against different time points after dilution gave an exponential first order kinetics from which k_4 was calculated. All kinetic values were determined using the software GraphPad Prism 4.

Molecular Modeling Studies. To derive a common binding-mode hypothesis, a combined docking and minimization approach was applied.

Docking studies were conducted with the program GOLD, version 5.2.2 (CCDC Software, http://www.ccdc.cam.ac.uk)[64] using the crystal structure PDB code 1P0I of human BChE (resolution 2.0 Å).[66] Prior to docking, all water molecules and non-protein atoms were removed and the amino acids were protonated with Protonate 3D in MOE[78] (version 2013.0801) at pH = 8 as the assay pH value. The binding site corresponding to the search region in the docking was defined by the following residues: Asn68, Asp70, Ser79, Trp82, Asn83, Gly115, Gly116, Gly117, Gln119, Thr120, Gly121, Thr122, Leu125, Tyr128, Glu197, Ser198, Ala199, Trp231, Leu286, Val288, Glu325, Ala328, Phe329, Tyr332, Trp430, His438, Gly439, Tyr440, Ile442.

Ligand structures were built in MOE or extracted from the crystal structure (ligand for redocking experiment, see below). The ligands were energy minimized in MOE with the MMFF94x force field to an rms gradient of 0.001 kcal/(mol·Å).

A redocking test was performed with the BChE crystal structure 4BDS (resolution, 2.10 Å) and tacrine as a reversible ligand. Tacrine was protonated at the acridinic N at pH = 8, according to a calculation with MoKa.[79] Fifty independent docking runs were carried out, with the number of operations set to 1 million to improve docking pose clustering. Among the four tested scoring functions, Goldscore[80,81] found the pose with the lowest rmsd (0.45 Å) to the crystal structure on higher ranks (rank 14) than the other functions (rank >40) and in a cluster containing 21 poses. The top pose showed an rmsd of 0.76 Å and was in a cluster with 27 poses. The Goldscore scoring function had previously proven to be applicable also in docking studies with AChE.[45,48]

Docking was performed with the same parameters (as used in the redocking test) for the kinetically investigated ligands listed in Table 2 (i.e., **2a**, **2c**, **2h**, **2i**, **2k**, **2l**, **2p**, **2s**, **2u**, **3a**, and **16**) as well as for ligand **1**, which possesses the most rigid structure. Chiral ligands were handled in both enantiomeric forms. The Goldscore value provided the first ranking criterion for the poses of a given ligand. In addition, rescoring with DSX[82] and CSD potentials were used as a second evaluation criterion. Moreover, docking poses were visually inspected, in particular the position of the carbamate moiety with respect to the catalytic serine and the orientation of the C═O group with respect to the oxyanion hole. Only poses showing a suitable orientation for the transfer of the carbamate to the serine were further considered.[83]

Ligand **1** as the most rigid compound showed well-clustered results and reasonable positions for carbamate transfer in both enantiomeric forms. The top rank for the *S*-enantiomer (second best in rescoring the top-five poses with DSX/CSD) and the second-best rank for the *R*-enantiomer (top rank in rescoring the top-five poses with DSX/CSD) showed the carbonyl oxygen of the carbamate pointing toward the oxyanion hole with distances of 2.7 and 2.8 Å between C═*O* and Gln117-*N* for the *S*- and the *R*-enantiomer, respectively. These poses were chosen as a reference for the binding modes of the studied class of compounds.

Because of the large size of the BChE binding pocket and the higher flexibility of the compounds in comparison to **1**, docking of all other investigated ligands resulted in more diverse and energetically rather degenerate poses besides the reference binding mode. To generate a more consistent binding-mode hypothesis, a modeling approach was followed for these structurally very similar ligands, in which the reference poses of compound **1** were used to construct the ligands in the binding site. Essentially, this was done with MOE 2014.0901 by deleting the methylene bridge of the tetracyclic structure of **1** and adding the required substituents to the aryl ring. The obtained structures were relaxed in the binding pocket with MiniMuDS[65] and scored with DSX/CSD.

For both enantiomers, the methyl group at the benzylic nitrogen was initially modeled in both the pseudo-equatorial and the pseudo-axial form. All *R*-enantiomers showed unfavorable distances of 2.1−2.4 Å between the axial methyl group and Gly116-Cα and were, hence, scored lower than the poses with the equatorial methyl. Thus, the *R*-enantiomers are presented with the methyl group in equatorial orientation. For the *S*-enantiomers, the methyl group in the axial position is much more favorable because it points to a small cavity between Trp82 of the choline binding site and His438 of the CAS. The conformer with the equatorial methyl group also fits to the binding site but corresponds to an energetically less favorable conformation, as investigated by force field calculations with the MMFF94s force field[84] in MOE. Accordingly, the *S*-enantiomers are presented with the methyl group in an axial orientation.

All figures of docking poses and enzyme structures were made with Pymol.[72]

Antioxidant Capacities (ORAC Assay). The antioxidant activity was determined by the oxygen radical absorbance capacity fluorescein (ORAC-FL) assay, modified by Dávalos et al.[85] The ORAC assay measures antioxidant scavenging activity against peroxyl radicals, their formation induced by 2,2′-azobis(2-amidinopropane) dihydrochloride (AAPH) at 37 °C. The reaction was carried out in 75 mM phosphate buffer (pH 7.4), and the final reaction mixture was 200 μL. Antioxidant (20 μL) and fluorescein (120 μL; 300 nM final concentration) were placed in the wells of a 96-well plate, and the mixture was incubated for 15 min at 37 °C. Then AAPH (Sigma, Steinheim, Germany) solution

DOI: 10.1021/acs.jmedchem.5b01674
J. Med. Chem. XXXX, XXX, XXX−XXX

(60 μL; 12 mM final concentration) was added rapidly. The plate was immediately placed into a SpectraFluor Plus plate reader (Tecan, Crailsheim, Germany) and fluorescence measured every 60 s for 90 min with excitation at 485 nm and emission at 535 nm. 6-Hydroxy-2,5,7,8-tetramethylchroman-2-carboxylic acid (Trolox, Sigma, Steinheim, Germany) was used as a standard (1−8 μM, final concentration). A blank (FL + AAPH) using phosphate buffer instead of antioxidant and Trolox calibration were carried out in each assay. The samples were measured at different concentrations (1−5 μM). All reaction mixtures were prepared 4-fold, and at least four independent runs were performed for each sample. Fluorescence measurements were normalized to the curve of the blank (without antioxidant). From the normalized curves, the area under the fluorescence decay curve (AUC) was calculated as

$$\mathrm{AUC} = 1 + \sum_{i=1}^{i=90} f_i / f_0$$

where f_0 is the initial fluorescence at 0 min and f_i is the fluorescence at time i. The net AUC for a sample was calculated as follows:

$$\text{net AUC} = \text{AUC antioxidant} - \text{AUC blank}$$

The ORAC-FL values were calculated:

$$\left[\frac{(\text{AUC sample}) - (\text{AUC blank})}{(\text{AUC Trolox}) - (\text{AUC blank})}\right]\left[\frac{\text{concentration of Trolox}}{\text{concentration of sample}}\right]$$

and expressed as Trolox equivalents by using the standard curve calculated for each assay. Final results were in μM of Trolox equivalent/μM of compound.

Neurotoxicity and Neuroprotection. Neurotoxicity and neuroprotection were done as described before.[47] HT 22 cells were derived from murine hippocampal tissue, kindly provided by the Max Planck Institute of Psychiatry, Munich, and were grown in high glucose Dulbecco's modified Eagle medium (DMEM, Invitrogen, Karlsruhe, Germany) supplemented with 10% (v/v) heat inactivated fetal calf serum (FCS) (Biochrom, Berlin, Germany). Cells were kept under standard cell culture conditions at 37 °C under 5% CO_2 in a humidified incubator and were subcultured every 2 d. Cell viability was determined by 3-(4,5-dimethylthiazol-2-yl)-2,5-diphenyltetrazolium bromide (MTT) assay. Briefly, cells were seeded in 96-well plates at a densitiy of 5 × 10 per well and cultured for 24 h. Subsequently cells were incubated for another 24 h with medium, compounds, or solvent in presence (neuroprotection assay) or absence (neurotoxicity assay) of 5 mM glutamate (monosodium L-glutamate, Merck, Darmstadt, Germany). Quercetin (Sigma, Steinheim, Germany) in a concentration of 25 μM served as the positive control in the neuroprotection assay. MTT (Sigma, Steinheim, Germany) solution (4 mg/mL in PBS) was diluted 1:10 with medium, and the mixture was added to the wells after removal of previous medium. The plates were then incubated for another 3 h. The supernatants were removed, and 100 μL of lysis buffer (10% SDS, pH 4.1) was added to the wells. Absorbance at 560 nM was determined on the next day with a multiwall plate photometer (Spectra Fluor Plus, Crailsheim, Germany). Results of cell viability are expressed as percentage to untreated control cells. All compounds were dissolved in DMSO and diluted with fresh medium. DMSO concentration in final dilutions was ≤0.1%. Data are expressed as the mean ± SD of at least three different independent experiments. Data were subjected to one way ANOVA followed by Dunnett's multiple comparison post-test using GraphPad Prism 4 software (levels of significance: (*) $p < 0.05$; (**) $p < 0.01$; (***) $p < 0.001$).

■ ASSOCIATED CONTENT

Supporting Information

The Supporting Information is available free of charge on the ACS Publications website at DOI: 10.1021/acs.jmedchem.5b01674.

Sequence comparison, IC_{50} values with confidence intervals, description and chromatograms of the enantiomeric separation of **2p**, energetic comparison of the enantiomeres, the postulated binding mode of **2l**, synthetic procedures and spectral data for **6b−d**, **7b−u**, **8a−c**, **9b−u**, **10a−c**, **2b−u**, and **3a−c** (PDF)

Molecular formula strings (CSV)

■ AUTHOR INFORMATION

Corresponding Author

*M.D.: phone, +0049-931 31-89676; fax, +0049-931 31-85494; e-mail, Michael.Decker@uni-wuerzburg.de.

Author Contributions

The manuscript was written with contributions of all authors. E.S. performed the synthesis and biological testing on AChE and BChE as well as the kinetic studies on BChE. S.W., under the supervision of C.S., was responsible for the molecular docking studies on BChE. B.K., under the supervision of J.H., tested the antioxidant capacity, neuroprotection, and toxicity of the synthesized compounds. J.W. performed the separation of enantiomers of **2p** under the supervision of G.B. M.D. was responsible for the supervision and development of the whole project.

Notes

The authors declare no competing financial interest.

■ ACKNOWLEDGMENTS

We gratefully acknowledge the German Science Foundation (DFG) for financial support (Grant DFG DE1546/6-1) as well as the German Academic National Foundation (Studienstiftung des Deutschen Volkes) for awarding a Ph.D. scholarship to S.W. We thank Gabriele Brunner for technical assistance on performing the ORAC assay.

■ ABBREVIATIONS USED

AAPH, 2,2′-azobis(2-amidinopropane) dihydrochloride; ATC, acetylthiocholine iodide; BTC, butyrylthiocholine iodide; CAS, catalytic active site; CD, circular dichroism; DIPEA, *N*,*N*-diisopropylethylamine; DMAc, dimethylacetamide; DTNB, 5,5′-dithiobis(2-nitrobenzoic acid); EC, Enzyme Commission number; *eq*BChE, equine butyrylcholinesterase; FL, fluorescein; GSH, glutathione; *h*AChE, human acetylcholinesterase; *h*BChE, human butyrylcholinesterase; MW, microwave; ORAC, oxygen radical absorbance capacity; rmsd, root mean square deviation; SAR, structure−activity relationship; TE, Trolox equivalent; Trolox, 6-hydroxy-2,5,7,8-tetramethylchroman-2-carboxylic acid

■ REFERENCES

(1) Wimo, A.; Prince, M. *World Alzheimer Report 2010. The Global Economic Impact of Dementia*; Alzheimer's Disease International, 2010.

(2) Prince, M.; Prina, M.; Guerchet, M. *World Alzheimer Report 2013. Journey of Caring. An Analysis of Long-Term Care for Dementia*; Alzheimer's Disease International, 2013.

(3) Querfurth, H. W.; LaFerla, F. M. Alzheimer's Disease. *N. Engl. J. Med.* **2010**, *362*, 329−344.

(4) Hensley, K. Neuroinflammation in Alzheimer's Disease: Mechanisms, Pathologic Consequences, and Potential for Therapeutic Manipulation. *J. Alzheimer's Dis.* **2010**, *21*, 1−14.

(5) Larson, M. E.; Lesné, S. E. Soluble Aβ Oligomer Production and Toxicity. *J. Neurochem.* **2012**, *120*, 125−139.

(6) Walsh, D. M.; Townsend, M.; Podlisny, M. B.; Shankar, G. M.; Fadeeva, J. V.; El Agnaf, O.; Hartley, D. M.; Selkoe, D. J. Certain Inhibitors of Synthetic Amyloidβ-Peptide (Aβ) Fibrillogenesis Block Oligomerization of Natural Aβ and Thereby Rescue Long-Term Potentiation. *J. Neurosci.* **2005**, *25*, 2455−2462.

DOI: 10.1021/acs.jmedchem.5b01674
J. Med. Chem. XXXX, XXX, XXX−XXX

(7) De Calignon, A.; Polydoro, M.; Suárez-Calvet, M.; William, C.; Adamowicz, D. H.; Kopeikina, K. J.; Pitstick, R.; Sahara, N.; Ashe, K. H.; Carlson, G. A.; Spires-Jones, T. L.; Hyman, B. T. Propagation of Tau Pathology in a Model of Early Alzheimer's Disease. *Neuron* **2012**, *73*, 685−697.
(8) Lee, H.; Perry, G.; Moreira, P. I.; Garrett, M. R.; Liu, Q.; Zhu, X.; Takeda, A.; Nunomura, A.; Smith, M. A. Tau Phosphorylation in Alzheimer's Disease: Pathogen or Protector? *Trends Mol. Med.* **2005**, *11*, 164−169.
(9) Eidenmüller, J.; Fath, T.; Hellwig, A.; Reed, J.; Sontag, E.; Brandt, R. Structural and Functional Implications of Tau Hyperphosphorylation: Information from Phosphorylation-Mimicking Mutated Tau Proteins. *Biochemistry* **2000**, *39*, 13166−13175.
(10) Khlistunova, I.; Biernat, J.; Wang, Y.; Pickhardt, M.; von Bergen, M.; Gazova, Z.; Mandelkow, E.; Mandelkow, E.-M. Inducible Expression of Tau Repeat Domain in Cell Models of Tauopathy. Aggregation is Toxic to Cells but can be Reversed by Inhibitor Drugs. *J. Biol. Chem.* **2006**, *281*, 1205−1214.
(11) Varadarajan, S.; Yatin, S.; Aksenova, M.; Butterfield, D. A. Review: Alzheimer's Amyloid β-Peptide-Associated Free Radical Oxidative Stress and Neurotoxicity. *J. Struct. Biol.* **2000**, *130*, 184−208.
(12) Wang, X.; Wang, W.; Li, Li.; Perry, G.; Lee, H.; Zhu, X. Oxidative Stress and Mitochondrial Dysfunction in Alzheimer's Disease. *Biochim. Biophys. Acta, Mol. Basis Dis.* **2014**, *1842*, 1240−1247.
(13) Francis, P. T. Glutamatergic Systems in Alzheimer's Disease. *Int. J. Geriatr. Psych.* **2003**, *18*, 15−21.
(14) Wenk, G. L. Neuropathologic Changes in Alzheimer's Disease: Potential Targets for Treatment. *J. Clin. Psychiatry* **2006**, *67*, 3−7.
(15) Francis, P. T.; Palmer, A. M.; Snape, M.; Wilcock, G. K. The Cholinergic Hypothesis of Alzheimer's Disease: A Review of Progress. *J. Neurol., Neurosurg. Psychiatry* **1999**, *66*, 137−147.
(16) Raina, P.; Santaguida, P.; Ismaila, A.; Patterson, C.; Cowan, D.; Levine, M.; Booker, L.; Oremus, M. Effectiveness of Cholinesterase Inhibitors and Memantine for Treating Dementia: Evidence Review for a Clinical Practice Guideline. *Ann. Intern. Med.* **2008**, *148*, 379−397.
(17) Rountree, S. D.; Chan, W.; Pavlik, V. N.; Darby, E. J.; Siddiqui, S.; Doody, R. S. Persistent Treatment with Cholinesterase Inhibitors and/or Memantine Slows Clinical Progression of Alzheimer Disease. *Alzheimer's Res. Ther.* **2009**, *1*, 7.
(18) Nordberg A.; Ballard C.; Bullock R.; Darreh-Shori T.; Somogyi, M. A Review of Butyrylcholinesterase as a Therapeutic Target in the Treatment of Alzheimer's Disease. *Prim. Care Companion CNS Disord.* **2013**, *15*, DOI: 10.4088/PCC.12r01412.
(19) Arendt, T.; Bruckner, M. K.; Lange, M.; Bigl, V. Changes in Acetylcholinesterase and Butyrylcholinesterase in Alzheimer's Disease Resemble Embryonic Development—A Study of Molecular Forms. *Neurochem. Int.* **1992**, *21*, 381−396.
(20) Giacobini, E. Cholinergic Function and Alzheimer's Disease. *Int. J. Geriatr. Psychiatry* **2003**, *18*, 1−5.
(21) Greig, N. H.; Utsuki, T.; Yu, Q.-S.; Zhu, X.; Holloway, H. W.; Perry, T.; Lee, B.; Ingram, D. K.; Lahiri, D. K. A New Therapeutic Target in Alzheimer's Disease Treatment: Attention to Butyrylcholinesterase. *Curr. Med. Res. Opin.* **2001**, *17*, 159−165.
(22) Grossberg, G. T. Cholinesterase Inhibitors for the Treatment of Alzheimer's Disease: Getting On and Staying On. *Curr. Ther. Res.* **2003**, *64*, 216−235.
(23) Darvesh, S.; Hopkins, D. A.; Geula, C. Neurobiology of Butyrylcholinesterase. *Nat. Rev. Neurosci.* **2003**, *4*, 131−138.
(24) Mesulam, M.-M.; Guillozet, A.; Shaw, P.; Levey, A.; Duysen, E. G.; Lockridge, O. Acetylcholinesterase Knockouts Establish Central Cholinergic Pathways and can Use Butyrylcholinesterase to Hydrolyze Acetylcholine. *Neuroscience* **2002**, *110*, 627−639.
(25) Hartmann, J.; Kiewert, C.; Duysen, E. G.; Lockridge, O.; Greig, N. H.; Klein, J. Excessive Hippocampal Acetylcholine Levels in Acetylcholinesterase-Deficient Mice are Moderated by Butyrylcholinesterase Activity. *J. Neurochem.* **2007**, *100*, 1421−1429.
(26) Furukawa-Hibi, Y.; Alkam, T.; Nitta, A.; Matsuyama, A.; Mizoguchi, H.; Suzuki, K.; Moussaoui, S.; Yu, Q.-S.; Greig, N. H.; Nagai, T.; Yamada, K. Butyrylcholinesterase Inhibitors Ameliorate Cognitive Dysfunction Induced by Amyloid-β Peptide in Mice. *Behav. Brain Res.* **2011**, *225*, 222−229.
(27) Greig, N. H.; Utsuki, T.; Ingram, D. K.; Wang, Y.; Pepeu, G.; Scali, C.; Yu, Q.-S.; Mamczarz, J.; Holloway, H. W.; Giordano, T.; Chen, D.; Furukawa, K.; Sambamurti, K.; Brossi, A.; Lahiri, D. K. Selective Butyrylcholinesterase Inhibition Elevates Brain Acetylcholine, Augments Learning and Lowers Alzheimer β-Amyloid Peptide in Roden. *Proc. Natl. Acad. Sci. U. S. A.* **2005**, *102*, 17213−17218.
(28) Maurice, T.; Strehaiano, M.; Siméon, N.; Bertrand, C.; Chatonnet, A. Learning Performances and Vulnerability to Amyloid Toxicity in the Butyrylcholinesterase Knockout Mouse. *Behav. Brain Res.* **2016**, *296*, 351−360.
(29) Li, B.; Duysen, E. G.; Lockridge, O. The Butyrylcholinesterase Knockout Mouse is Obese on a High-Fat Diet. *Chem.-Biol. Interact.* **2008**, *175*, 88−91.
(30) Iwasaki, T.; Yoneda, M.; Nakajima, A.; Terauchi, Y. Serum Butyrylcholinesterase is Strongly Associated with Adiposity, the Serum Lipid Profile and Insulin Resistance. *Intern. Med.* **2007**, *46*, 1633−1639.
(31) Sato, K. K.; Hayashi, T.; Maeda, I.; Koh, H.; Harita, N.; Uehara, S.; Onishi, Y.; Oue, K.; Nakamura, Y.; Endo, G.; Kambe, H.; Fukuda, K. Serum Butyrylcholinesterase and the Risk of Future Type 2 Diabetes: the Kansai Healthcare Study. *Clin. Endocrinol.* **2014**, *80*, 362−367.
(32) Stojanov, M.; Stefanović, A.; Džingalašević, G.; Mandić-Radić, S.; Prostran, M. Butyrylcholinesterase Activity in Young Men and Women: Association with Cardiovascular Risk Factors. *Clin. Biochem.* **2011**, *44*, 623−626.
(33) Alcântara, V. M.; Chautard-Freire-Maia, E. A.; Scartezini, M.; Cerci, M. S. J.; Braun-Prado, K.; Picheth, G. Butyrylcholinesterase Activity and Risk Factors for Coronary Artery Disease. *Scand. J. Clin. Lab. Invest.* **2002**, *62*, 399−404.
(34) Dougherty, D. A.; Stauffer, D. A. Acetylcholine Binding by a Synthetic Receptor: Implications for Biological Recognition. *Science* **1990**, *250*, 1558−1560.
(35) Brus, B.; Košak, U.; Turk, S.; Pišlar, A.; Coquelle, N.; Kos, J.; Stojan, J.; Colletier, J.-P.; Gobec, S. Discovery, Biological Evaluation, and Crystal Structure of a Novel Nanomolar Selective Butyrylcholinesterase Inhibitor. *J. Med. Chem.* **2014**, *57*, 8167−8179.
(36) Huang, G.; Kling, B.; Darras, F. H.; Heilmann, J.; Decker, M. Identification of a Neuroprotective and Selective Butyrylcholinesterase Inhibitor Derived from the Natural Alkaloid Evodiamine. *Eur. J. Med. Chem.* **2014**, *81*, 15−21.
(37) Takahashi, J.; Hijikuro, I.; Kihara, T.; Murugesh, M. G.; Fuse, S.; Tsumura, Y.; Akaike, A.; Niidome, T.; Takahashi, T.; Sugimoto, H. Design, Synthesis and Evaluation of Carbamate-Modified (−)-N^1-Phenethylnorphysostigmine Derivatives as Selective Butyrylcholinesterase Inhibitors. *Bioorg. Med. Chem. Lett.* **2010**, *20*, 1721−1723.
(38) Groner, E.; Ashani, Y.; Schorer-Apelbaum, D.; Sterling, J.; Herzig, Y.; Weinstock, M. The Kinetics of Inhibition of Human Acetylcholinesterase and Butyrylcholinesterase by Two Series of Novel Carbamates. *Mol. Pharmacol.* **2007**, *71*, 1610−1617.
(39) Yu, Q.; Greig, N. H.; Holloway, H. W.; Brossi, A. Syntheses and Anticholinesterase Activities of (3a*S*)-*N*1, *N*8-Bisnorphenserine, (3a*S*)-*N1*,*N8*-Bisnorphysostigmine, their Antipodal Isomers, and Other Potential Metabolites of Phenserine. *J. Med. Chem.* **1998**, *41*, 2371−2379.
(40) Darvesh, S.; Darvesh, K. V.; McDonald, R. S.; Mataija, D.; Walsh, R.; Mothana, S.; Lockridge, O.; Martin, E. Carbamates with Differential Mechanism of Inhibition Toward Acetylcholinesterase and Butyrylcholinesterase. *J. Med. Chem.* **2008**, *51*, 4200−4212.
(41) Chiou, S.-Y.; Huang, C.-F.; Hwang, M.-T.; Lin, G. Comparison of Active Sites of Butyrylcholinesterase and Acetylcholinesterase Based on Inhibition by Geometric Isomers of Benzene-di-*N*-Substituted Carbamates. *J. Biochem. Mol. Toxicol.* **2009**, *23*, 303−308.
(42) Lin, G.; Lee, Y.-R.; Liu, Y.-C.; Wu, Y.-G. *Ortho* Effects for Inhibition Mechanisms of Butyrylcholinesterase by *o*-Substituted Phenyl *N*-Butyl Carbamates and Comparison with Acetylcholinesterase, Cholesterol Esterase, and Lipase. *Chem. Res. Toxicol.* **2005**, *18*, 1124−1131.

DOI: 10.1021/acs.jmedchem.5b01674
J. Med. Chem. XXXX, XXX, XXX−XXX

(43) Carolan, C. G.; Dillon, G. P.; Khan, D.; Ryder, S. A.; Gaynor, J. M.; Reidy, S.; Marquez, J. F.; Jones, M.; Holland, V.; Gilmer, J. F. Isosorbide-2-benzyl Carbamate-5-salicylate, A Peripheral Anionic Site Binding Subnanomolar Selective Butyrylcholinesterase Inhibitor. *J. Med. Chem.* **2010**, *53*, 1190−1199.
(44) Decker, M.; Krauth, F.; Lehmann, J. Novel Tricyclic Quinazolinimines and Related Tetracyclic Nitrogen Bridgehead Compounds as Cholinesterase Inhibitors with Selectivity Towards Butyrylcholinesterase. *Bioorg. Med. Chem.* **2006**, *14*, 1966−1977.
(45) Darras, F. H.; Wehle, S.; Huang, G.; Sotriffer, C. A.; Decker, M. Amine Substitution of Quinazolinones Leads to Selective Nanomolar AChE Inhibitors with 'Inverted' Binding Mode. *Bioorg. Med. Chem.* **2014**, *22*, 4867−4881.
(46) Decker, M. Homobivalent Quinazolinimines as Novel Nanomolar Inhibitors of Cholinesterases with Dirigible Selectivity Toward Butyrylcholinesterase. *J. Med. Chem.* **2006**, *49*, 5411−5413.
(47) Darras, F. H.; Kling, B.; Heilmann, J.; Decker, M. Neuroprotective Tri- and Tetracyclic BChE Inhibitors Releasing Reversible Inhibitors upon Carbamate Transfer. *ACS Med. Chem. Lett.* **2012**, *3*, 914−919.
(48) Darras, F. H.; Pockes, S.; Huang, G.; Wehle, S.; Strasser, A.; Wittmann, H.-J.; Nimczick, M.; Sotriffer, C. A.; Decker, M. Synthesis, Biological Evaluation, and Computational Studies of Tri- and Tetracyclic Nitrogen-Bridgehead Compounds as Potent Dual-Acting AChE Inhibitors and hH$_3$ Receptor Antagonists. *ACS Chem. Neurosci.* **2014**, *5*, 225−242.
(49) Sawatzky, E.; Bukowczan, J.; Decker, M. Investigation into Selective Debenzylation and Ring Cleavage of Quinazoline Based Heterocycles. *Tetrahedron Lett.* **2014**, *55*, 2973−2976.
(50) Zhao, D.; Shen, Q.; Zhou, Y.-R.; Li, J.-X. KO*t*Bu-Mediated Stereoselective Addition of Quinazolines to Alkynes Under Mild Conditions. *Org. Biomol. Chem.* **2013**, *11*, 5908−5912.
(51) Ellman, G. L. A Colorimetric Method for Determining Low Concentrations of Mercaptans. *Arch. Biochem. Biophys.* **1958**, *74*, 443−450.
(52) Ellman, G. L.; Courtney, K. D.; Andres, V.; Featherstone, R. M. A New and Rapid Colorimetric Determination of Acetylcholinesterase Acticity. *Biochem. Pharmacol.* **1961**, *7*, 88−95.
(53) Yücel, Y. Y.; Tacal, Ö.; Özer, I. Comparative Effects of Cationic Triarylmethane, Phenoxazine and Phenothiazine Dyes on Horse Serum Butyrylcholinesterase. *Arch. Biochem. Biophys.* **2008**, *478*, 201−205.
(54) Topliss, J. G. Utilization of Operational Schemes for Analog Synthesis in Drug Design. *J. Med. Chem.* **1972**, *15*, 1006−1011.
(55) O'Boyle, N. M.; Bostrom, J.; Sayle, R. A.; Gill, A. Using Matched Molecular Series as a Predictive Tool to Optimize Biological Activity. *J. Med. Chem.* **2014**, *57*, 2704−2713.
(56) Kier, L. B.; Hall, L. H. Bioisosterism: Quantitation of Structure and Property Effects. *Chem. Biodiversity* **2004**, *1*, 138−151.
(57) Sheridan, R. P. The Most Common Chemical Replacements in Drug-Like Compounds. *J. Chem. Inf. Model.* **2002**, *42*, 103−108.
(58) Cheung, J.; Rudolph, M. J.; Burshteyn, F.; Cassidy, M. S.; Gary, E. N.; Love, J.; Franklin, M. C.; Height, J. J. Structures of Human Acetylcholinesterase in Complex with Pharmacologically Important Ligands. *J. Med. Chem.* **2012**, *55*, 10282−10286.
(59) Harel, M.; Schalk, I.; Ehret-Sabatier, L.; Bouet, F.; Goeldner, M.; Hirth, C.; Axelsen, P. H.; Silman, I.; Sussman, J. L. Quaternary Ligand Binding to Aromatic Residues in the Active-Site Gorge of Acetylcholinesterase. *Proc. Natl. Acad. Sci. U. S. A.* **1993**, *90*, 9031−9035.
(60) Dvir, H.; Wong, D. M.; Harel, M.; Barril, X.; Orozco, M.; Luque, F. J.; Muñoz-Torrero, D.; Camps, P.; Rosenberry, T. L.; Silman, I.; Sussman, J. L. 3D Structure of Torpedo californica Acetylcholinesterase Complexed with Huprine X at 2.1 Å Resolution: Kinetic and Molecular Dynamic Correlates. *Biochemistry* **2002**, *41*, 2970−2981.
(61) Bar-On, P.; Millard, C. B.; Harel, M.; Dvir, H.; Enz, A.; Sussman, J. L.; Silman, I. Kinetic and Structural Studies on the Interaction of Cholinesterases with the Anti-Alzheimer Drug Rivastigmine. *Biochemistry* **2002**, *41*, 3555−3564.
(62) Hosie, L.; Sutton, L. D.; Quinn, D. M. *p*-Nitrophenyl and Cholesteryl-*N*-Alkyl Carbamates as Inhibitors of Cholesterol Esterase. *J. Biol. Chem.* **1987**, *262*, 260−264.
(63) Feaster, S. R.; Lee, K.; Baker, N.; Hui, D. Y.; Quinn, D. M. Molecular Recognition by Cholesterol Esterase of Active Site Ligands: Structure-Reactivity Effects for Inhibition by Aryl Carbamates and Subsequent Carbamylenzyme Turnover. *Biochemistry* **1996**, *35*, 16723−16734.
(64) *GOLD Suite*, version 5.2.2; CCDC Software: Cambridge, U.K.; http://www.ccdc.cam.ac.uk. Jones, G.; Willett, P.; Glen, R. C.; Leach, A. R.; Taylor, R. Development and Validation of a Genetic Algorithm for Flexible Docking. *J. Mol. Biol.* **1997**, *267*, 727−748.
(65) Spitzmüller, A.; Velec, H. F. G.; Klebe, G. MiniMuDS: A New Optimizer using Knowledge-Based Potentials Improves Scoring of Docking Solutions. *J. Chem. Inf. Model.* **2011**, *51*, 1423−1430.
(66) Nicolet, Y.; Lockridge, O.; Masson, P.; Fontecilla-Camps, J. C.; Nachon, F. Crystal Structure of Human Butyrylcholinesterase and of its Complexes with Substrate and Products. *J. Biol. Chem.* **2003**, *278*, 41141−41147.
(67) www.rcsb.org. Berman, H. M.; Westbrook, J.; Feng, Z.; Gilliland, G.; Bhat, T. N.; Weissig, H.; Shindyalov, I. N.; Bourne, P. E. The Protein Data Bank. *Nucleic Acids Res.* **2000**, *28*, 235−242.
(68) Nawaz, S.; Ayaz, M.; Brandt, W.; Wessjohann, L. A.; Westermann, B. Cation-π and π-π Stacking Interactions Allow Selective Inhibition of Butyrylcholinesterase by Modified Quinine and Cinchonidine Alkaloids. *Biochem. Biophys. Res. Commun.* **2011**, *404*, 935−940.
(69) Karlsson, D.; Fallarero, A.; Brunhofer, G.; Mayer, C.; Prakash, O.; Mohan, C. G.; Vuorela, P.; Erker, T. The Exploration of Thienothiazines as Selective Butyrylcholinesterase Inhibitors. *Eur. J. Pharm. Sci.* **2012**, *47*, 190−205.
(70) Basiri, A.; Murugaiyah, V.; Osman, H.; Kumar, R. S.; Kia, Y.; Hooda, A.; Parsons, R. B. Cholinesterase Inhibitory Activity Versus Aromatic Core Multiplicity: A Facile Green Synthesis and Molecular Docking Study of Novel Piperidine Embedded Thiazolopyrimidines. *Bioorg. Med. Chem.* **2014**, *22*, 906−916.
(71) Gao, D.; Zhan, C.-G. Modeling Effects of Oxyanion Hole on the Ester Hydrolysis Catalyzed by Human Cholinesterases. *J. Phys. Chem. B* **2005**, *109*, 23070−23076.
(72) *The PyMOL Molecular Graphics System*, version 1.7.4.3; Schrödinger, LLC.
(73) Berdagué, P.; Herbert-Pucheta, J.-E.; Jha, V.; Panossian, A.; Leroux, F. R.; Lesot, P. Multi-nuclear NMR of Axially Chiral Biaryls in Polypeptide Orienting Solvents: Spectral Discriminations and Enantiorecognition Mechanisms. *New J. Chem.* **2015**, *39*, 9504−9517.
(74) Lewerenz, J.; Hewett, S. J.; Huang, Y.; Lambros, M.; Gout, P. W.; Kalivas, P. W.; Massie, A.; Smolders, I.; Methner, A.; Pergande, M.; Smith, S. B.; Ganapathy, V.; Maher, P. The Cystine/Glutamate Antiporter System x_c^- in Health and Disease: From Molecular Mechanisms to Novel Therapeutic Opportunities. *Antioxid. Redox Signaling* **2013**, *18*, 522−555.
(75) Murphy, T. H.; Miyamoto, M.; Sastre, A.; Schnaar, R.; Coyle, J. T. Glutamate Toxicity in a Neuronal Cell Line Involves Inhibition of Cystine Transport Leading to Oxidative Stress. *Neuron* **1989**, *2*, 1547−1558.
(76) Fukui, M.; Song, J.-H.; Choi, J.; Choi, H. J.; Zhu, B. T. Mechanism of Glutamate-Induced Neurotoxicity in HT22 Mouse Hippocampal Cells. *Eur. J. Pharmacol.* **2009**, *617*, 1−11.
(77) Tan, S.; Wood, M.; Maher, P. Oxidative Stress Induces a Form of Programmed Cell Death with Characteristics of Both Apoptosis and Necrosis in Neuronal Cells. *J. Neurochem.* **1998**, *71*, 95−105.
(78) *Molecular Operating Environment (MOE)*, versions 2013.0801 and 2014.0901; Chemical Computing Group (1010 Sherbooke St. West, Suite No. 910, Montreal, QC, H3A 2R7, Canada), 2011.
(79) Milletti, F.; Storchi, L.; Sforna, G.; Cruciani, G. J. New and Original pK_a Prediction Method Using Grid Molecular Interaction Fields. *J. Chem. Inf. Model.* **2007**, *47*, 2172−2181.
(80) Jones, G.; Willett, P.; Glen, R. C. Molecular Recognition of Receptor Sites Using a Genetic Algorithm with a Description of Desolvation. *J. Mol. Biol.* **1995**, *245*, 43−53.
(81) Jones, G.; Willett, P.; Glen, R. C.; Leach, A. R.; Taylor, R. Development and Validation of a Genetic Algorithm for Flexible Docking. *J. Mol. Biol.* **1997**, *267*, 727−748.

DOI: 10.1021/acs.jmedchem.5b01674
J. Med. Chem. XXXX, XXX, XXX−XXX

(82) Neudert, G.; Klebe, G. DSX: A Knowledge-Based Scoring Function for the Assessment of Protein-Ligand Complexes. *J. Chem. Inf. Model.* **2011**, *51*, 2731−2745.
(83) Bartolucci, C.; Siotto, M.; Ghidini, E.; Amari, G.; Bolzoni, P. T.; Racchi, M.; Villetti, G.; Delcanale, M.; Lamba, D. Structural Determinants of *Torpedo californica* Acetylcholinesterase Inhibition by the Novel and Orally Active Carbamates Based Anti-Alzheimer Drug Ganstigmine (CHF-2819). *J. Med. Chem.* **2006**, *49*, 5051−5058.
(84) Halgren, T. A. Merck Molecular Force Field. I. Basis, Form, Scope, Parameterization, and Performance of MMFF94. *J. Comput. Chem.* **1996**, *17*, 490−510.
(85) Dávalos, A.; Gómez-Cordovés, C.; Bartolomé, B. Extending Applicability of the Oxygen Radical Absorbance Capacity (ORAC−Fluorescein) Assay. *J. Agric. Food Chem.* **2004**, *52*, 48−54.

DOI: 10.1021/acs.jmedchem.5b01674
J. Med. Chem. XXXX, XXX, XXX−XXX